Investigating the limiting aircraft design-dependent and environmental factors of persistent contrail formation

Liam Megill[1, 2] and Volker Grewe[1, 2]

[1]Deutsches Zentrum für Luft- und Raumfahrt, Institut für Physik der Atmosphäre, Oberpfaffenhofen, Germany
[2]Delft University of Technology, Faculty of Aerospace Engineering, Section Aircraft Noise and Climate Effects, Delft, The Netherlands

Correspondence: Liam Megill (liam.megill@dlr.de)

Abstract. Mounting evidence has highlighted the role of aviation non-CO_2 emissions in contributing to anthropogenic climate change. Of particular importance is the impact of ~~aircraft contrails and induced cloudiness~~contrails, which recent studies attribute to over one third of the total ~~Effective Radiative Forcing~~ effective radiative forcing from aircraft operations. However, the relative importance of the aircraft design-dependent and environmental factors that influence ~~and limit~~ the formation of persistent contrails is not yet well understood. In this paper, we use ERA5 data from the 2010 decade to better understand the interplay between the factors on a climatological timescale. We identify ice supersaturation as the most limiting factor for all considered aircraft designs, underscoring the importance of accurately estimating ice supersaturated regions. We also develop climatological relationships that describe potential persistent contrail formation as a function of the pressure level and Schmidt-Appleman mixing line slope~~G, and~~. We find that the influence of aircraft design on persistent contrail formation reduces with increasing altitude. ~~Globally-averaged persistent contrail formation could increase by 13.8 % for next generation conventional aircraft , or by 71.4 % if all aircraft were to be replaced by hydrogen combustion or fuel cell equivalents. On the other hand,~~ Compared to a state-of-the-art conventional aircraft with an overall propulsion system efficiency of 0.37, envisioned water vapour extraction technologies ~~such as the Water Enhanced Turbofan concept~~ have the potential to reduce persistent contrail formation by ~~53.6 %to 85.6 % . The introduction of~~ up to 85.1 %. On the other hand, compared to the same reference, hydrogen combustion and fuel cell aircraft could increase globally-averaged persistent contrail formation by 46.5 and 54.7 % respectively. Due to differing contrail properties, further work is required to translate these changes into climate impacts. This study is a step towards the development of a new, computationally inexpensive method to analyse the contrail climate impact of novel aviation fuels and propulsion technologies~~, therefore, present both challenges and opportunities with respect to persistent contrail formation~~.

1 Introduction

Aviation contributes to anthropogenic climate change through ~~CO$_2$~~ carbon dioxide (CO$_2$) emissions and non-CO$_2$ emissions and effects. Of particular importance is the formation of condensation trails, or contrails, which can form behind aircraft. ~~Although most~~ Most contrails quickly dissipate and have ~~no effect~~ a negligible impact on the climate~~.~~. However, in certain ambient conditions~~,~~ contrails can spread to form contrail-cirrus clouds and persist for many hours (Haywood et al., 2009; Schumann and Heymsfield, 2017). Current best estimates suggest that contrails and the resulting ~~increase in~~ aircraft-induced cloudiness could be responsible for around a half of the anthropogenic ~~Effective Radiative Forcing~~ effective radiative forcing in 2018 stemming from aircraft operations between 1940 and 2018 (Lee et al., 2021), although these estimates are highly uncertain ~~(Kärcher, 2018; Lee et al., 2021; Burkhardt and Kärcher, 2011)~~(Burkhardt and Kärcher, 2011; Kärcher, 2018; Lee et al., 2021). As aircraft using alternative aviation fuels ~~such as Sustainable Aviation Fuels (SAFs) and hydrogen (H$_2$)~~ are proposed and developed, there is a need to more closely examine their potential contrail climate impact.

Contrails ~~are formed~~ can form when the hot and moist aircraft engine exhaust plume ~~expands~~ mixes with the ambient air and cools. If, during ~~expansion~~mixing, the exhaust plume becomes supersaturated with respect to liquid water, water vapour condenses around ~~ice~~ condensation nuclei in the exhaust, primarily soot (Kärcher and Yu, 2009; Kärcher et al., 2015). If the ambient temperature is below the homogeneous freezing temperature, the water droplets freeze to form ice crystals, creating a visible contrail. These conditions together constitute the Schmidt-Appleman Criterion ~~(SAC, Schumann, 1996; Schmidt, 1941; Appleman, 1953)~~ (SAC, Schumann, 1996; see also Schmidt, 1941; Appleman, 1953). A lack of ice nuclei in the exhaust does not prevent a contrail from forming or persisting: In very low soot or soot-free conditions, ~~for example behind aircraft using SAF or H$_2$ respectively,~~ volatile exhaust particles and ambient, natural or anthropogenic aerosols can also activate into water droplets ~~(Yu et al., 2024; Kärcher et al., 2015; Bier and Burkhardt, 2019; Kärcher, 2018)~~(Kärcher et al., 2015; Kärcher, 2018; Bier and Burkhardt,. However, due to the large variability in the properties and concentration of the ambient aerosols (e.g. Brock et al., 2021; Voigt et al., 2022), the resulting ice crystal number and radiative effect of the subsequent contrails are currently highly uncertain.

Contrails can persist for many hours if the ambient conditions are supersaturated with respect to ice (Haywood et al., 2009). These contrails slowly ~~sink and spread outdue to wind shear, forming contrail cirrus and often mixing~~ spread out, transitioning into contrail cirrus that can merge with natural cirrus and be transported over large distances (Kärcher, 2018). Contrail cirrus ~~reflect~~ scatter incoming shortwave radiation and ~~trap~~ reduce outgoing longwave radiation (Kärcher, 2018). The radiative effect of contrail cirrus is thus diurnal in nature, with contrails warming during the night and both warming and cooling during the day (Meerkötter et al., 1999). However, on average, the warming effect has been shown to dominate ~~(Meerkötter et al., 1999; Grewe et al., 2017b; Lee et al., 2021)~~(Grewe et al., 2017b; Lee et al., 2021).

Recent studies have shown that a small number of flights ~~have an over-proportional contrail warming effect~~ can have an outsize contribution to the total warming from contrail cirrus (e.g. Grewe et al., 2014; Teoh et al., 2020, 2022a). Avoiding contrail formation, in particular the so-called "big hits", is a topic of ongoing research ~~(e.g. Sausen et al., 2024; Gierens et al., 2008; Filippone,~~ (e.g. Gierens et al., 2008; Filippone, 2015; Rosenow and Fricke, 2019; Sausen et al., 2024). Several open questions should be addressed before contrail avoidance is routinely used in daily operations (Grewe et al., 2017c). One significant hindrance to

contrail avoidance schemes is that although contrail formation can be reliably forecasted, persistence currently cannot (Gierens et al., 2020; Wilhelm et al., 2022; Hofer et al., 2024b).

With this research, we take a more holistic approach to the ~~persistent contrail formation~~ formation of persistent contrails, focusing on the development of longer-term strategies rather than individual contrail avoidance. We aim to better understand the interplay between aircraft-dependent and -independent factors which limit persistent contrail formation on a climatological timescale. Persistent contrail formation can be limited by three main factors: droplet formation, droplet freezing and persistence. Our objectives are 1) to identify which factor(s) is/are generally responsible for the boundaries of persistent contrail formation regions; 2) determine the altitude-, latitude- and seasonal dependence of these factors and of persistent contrail formation regions; and 3) explore possibilities for the targeted introduction of future aircraft designs to reduce persistent contrail formation. This study is thus a step towards the development of a new, computationally inexpensive method to analyse the contrail climate impact of novel aircraft fuels and propulsion technologies. Next to conventional kerosene, we consider the following technologies: Sustainable Aviation Fuels (SAFs), hydrogen (H_2) fuel cells and combustion, hybrid-electric aircraft and ~~the Water-Enhanced Turbofan (WET) concept (Schmitz et al., 2021)~~water vapour extraction technologies. We describe the potential contrail impacts of each technology briefly below.

SAFs have the potential to reduce the climate impact of aviation in the shorter term. The most obvious benefit of using such fuels is the reduction of lifecycle CO_2 emissions, but SAF usage may also affect the formation and climate impact of contrails. SAFs tend to have a higher ~~H/C~~ hydrogen-to-carbon ratio and lower proportion of aromatics compared to conventional kerosene. This results in a lower soot and ice crystal number concentration (Moore et al., 2017; Bräuer et al., 2021b; Voigt et al., 2021), which in turn reduces the optical depth and climate impact of contrails (Burkhardt et al., 2018). However, the higher ~~H/C~~ hydrogen-to-carbon ratio also results in increased water vapour emissions and thus to the more frequent formation of persistent contrails ~~(Rojo et al., 2015; Caiazzo et al., 2017; Hofer et al., 2024a; Teoh et al., 2022b)~~ (Rojo et al., 2015; Caiazzo et al., 2017; Teoh et al., 2022b; Hofer et al., 2024a).

In the longer term, another promising technology is hydrogen, either combusted in a jet engine or used in a fuel cell. The use of hydrogen has no direct CO_2 emissions and, unlike conventional jet fuels, is not expected to produce any soot or particulate emissions, although the formation of ultrafine volatile particles from lubricant oil vapours has been observed in ~~lab~~ laboratory combustion tests (Ungeheuer et al., 2022). The use of H_2 in a jet engine will also significantly increase water vapour emissions, from 1.25 kg~~/kg~~ kg^{-1}(kerosene) for conventional kerosene to around 8.94 kg~~/kg~~ kg^{-1}(hydrogen). Taking into account that H_2 has a gravimetric energy density around 3 times higher than kerosene - 120.9 compared to 43.6 MJ~~/kg~~ kg^{-1} - the slope of the SAC mixing line is around 2.6 times larger for H_2 combustion than for kerosene for the same overall propulsion system efficiency. Given the low exhaust temperature, that factor is even higher for H_2 fuel cells, between 2.7 and 8.2 times, depending on the operating voltage of the fuel cell (Gierens, 2021). We can, therefore, expect a significant increase in contrail formation from H_2 aircraft (e.g. Grewe et al., 2017a; Kaufmann et al., 2024). However, recent studies ~~(Sanogo et al., 2024; Wolf et al., 2023)~~ (Wolf et al., 2023; Sanogo et al., 2024) show that contrail formation does not scale linearly with this factor. Kaufmann et al. (2024) in particular show that contrail formation from hydrogen-powered aircraft is strongly dependent on season, altitude

and latitude. This suggests that the ambient atmospheric conditions and processes, rather than the aircraft design, mostly limit persistent contrail formation.

Other technologies reduce the slope of the mixing line, promising less frequent contrail formation - here we consider hybrid-electric aircraft and the Water-Enhanced Turbofan (WET) concept. Hybrid-electric aircraft are promising in that they could be flown such that only electric power is used within regions of potential persistent contrail formation. Even when electric power is combined with conventional fuel during continuous use, the mixing line slope of the combined system is lower, resulting in fewer contrails forming (Yin et al., 2020). However, ~~hybrid electric~~ hybrid-electric aircraft have a limited use case due to their low speed and service ceiling. Another possibility for reducing the mixing line slope is by condensing, storing and releasing water in areas in which the ambient conditions are not conducive to persistent contrail formation. A notable example of this is the WET concept (Schmitz et al., 2021; Pouzolz et al., 2021; Kaiser et al., 2022). The benefit of such a system is that it can be integrated into a wider range of aircraft and is not limited by speed and service ceiling.

In the following section, we describe the methodology and data used in this study. The resulting limiting factors of climatological persistent contrail formation are analysed, discussed and compared to one another in Section 3. We conclude the study ~~with~~ in Section 4.

2 Data and methods

This section outlines the data and methods used to calculate the limiting factors of persistent contrail formation on a climatological basis. Section 2.1 describes the thermodynamic contrail formation and persistence criteria ~~,~~ and provides the calculation methods for the mixing line slopes of various propulsion systems. We cover the full range of possible mixing line slopes, but also specify certain aircraft designs for easier comparison between different technologies, which are described in Section 2.2. We provide an overview of our air traffic scenario in Section 2.3~~; the European Centre for Medium-Range Weather Forecasts (ECMWF) ERA5 dataset (Hersbach et al., 2020)~~. In Section 2.4, we present the reanalysis dataset and the corresponding humidity corrections used in this study~~in Section 2.4~~. Finally, the limiting factors and maximum slope analyses are described in Sections 2.5 and 2.7 respectively.

2.1 Contrail formation and persistence

As described in the introduction, contrails form as ~~a result of isobaric mixing of~~ the hot and moist aircraft engine exhaust plume mixes with the cold and dry ambient air. The mixing process ~~can be thermodynamically approximated by connecting the exhaust and ambient conditions with a straight~~ is approximated by Schmidt-Appleman theory (Schumann, 1996) as isobaric mixing, resulting in a straight mixing line on a temperature vs. water vapour partial pressure diagram ~~, such as Figure 1 (gray dashed lines~~ (e.g. the dashed lines in Figure 1). The slope G of the mixing line is a function of the ambient pressure as well as aircraft engine and fuel-dependent properties. For conventional kerosene (CON), the slope can be calculated using the following equation (Schumann, 1996),
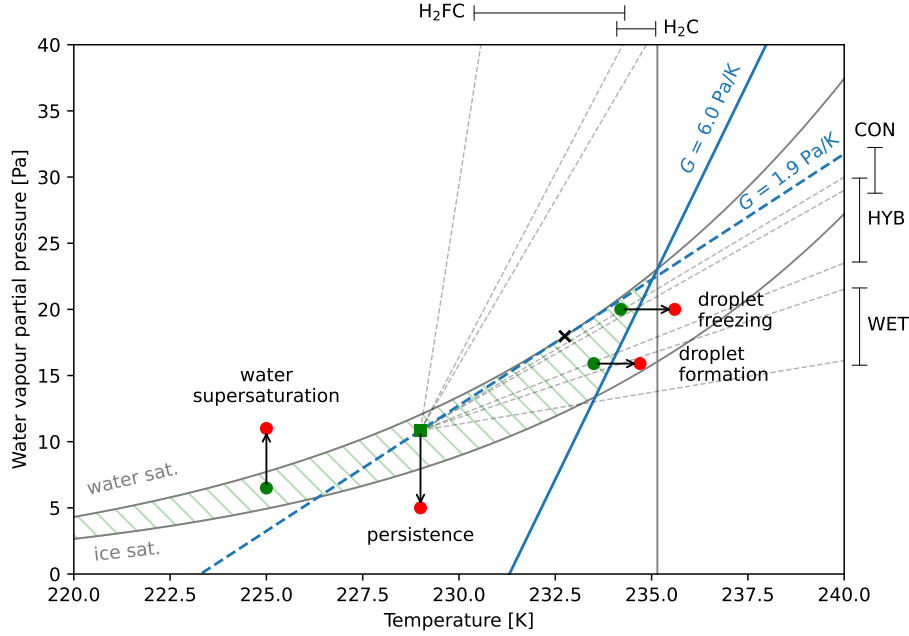
Figure 1. Ambient temperature vs. water vapour partial pressure diagram with an example threshold mixing line for an aircraft with ~~$G = 3.7$~~ $G = 6.0$ Pa~~/~~ K^{-1} (blue line). A persistent contrail would form behind this aircraft if the ambient conditions are within the green hashed area. Four limiting factors can be identified that define this area, represented by the arrows from green (persistent contrail forms) to red (persistent contrail does not form) points. Ranges of mixing line slopes for each aircraft type at 250 hPa (FL340) are shown with dotted lines. The dashed blue line $G = 1.9$ Pa K^{-1} is the threshold mixing line for the ambient condition defined by the green square. The point at which this mixing line is tangential to the water saturation curve (T_{max}, see main text) is shown by a black cross.

$$G_{\underline{CON}\text{CON}} = \frac{c_p p_a}{\epsilon} \frac{EI_{H_2O}}{(1 - \eta) Q} \tag{1}$$

where ~~$e_p = 1004$ J/kg/K~~ $c_p = 1004$ J kg^{-1} K^{-1} is the isobaric heat capacity of air, p_a the ambient pressure [Pa], $\epsilon = 0.622$ the molar mass ratio of water vapour and dry air, EI_{H_2O} the emission index of water vapour [kg~~/kg~~ kg^{-1}(fuel)], η the overall propulsion system efficiency ~~,~~ and Q the lower heating value of the fuel [MJ~~/kg~~ kg^{-1}].

This definition was adapted by Yin et al. (2020) to parallel hybrid battery-electric aircraft by introducing a ratio R, where $R = 1$ is pure liquid fuel operation and $R = 0$ is pure electric operation. The quasi-electric energy content Q_E^0 is defined as $Q(\eta_K / \eta_E)$, where K refers to liquid fuel (kerosene) ~~,~~ and E to the electric system.

$$G_{\underline{HYB}\text{HYB}} = \frac{c_p p_a}{\epsilon} \frac{R \cdot EI_{H_2O}}{R(1 - \eta_K) Q + (1 - R)(1 - \eta_E) Q_E^0} \tag{2}$$

The definition was further modified for hydrogen combustion (~~H₂~~H₂C) and fuel cell (~~H₂~~H₂FC) aircraft by Gierens (2021). Eq. (3) is very similar to the standard definition and is used for hydrogen combustion, where ~~$|\Delta h| = 120.9$ MJ/kg~~the lower heating value $|\Delta h| = 120.9\,\text{MJ kg}^{-1}$:

$$G_{\underline{H_2C}\,\text{H}_2\text{C}} = \frac{c_p p_a}{\epsilon} \frac{EI_{H_2O}}{(1-\eta)|\Delta h|} \tag{3}$$

The calculation for fuel cells is more complex. Fuel cells operate in conjunction with electric motors, which fully decouples the exhaust from the propulsion. The exhaust could be modified to recover heat, separate and store water or achieve a desired ice crystal size. The properties of contrails produced by fuel cell powered aircraft thus depend on the design of the fuel cell system to a much larger degree than for traditional gas turbine engines. Moreover, due to the potentially very high supersaturations reached in the plume, homogeneous droplet nucleation could also take place even without the presence of aerosols. However, there is not yet a common understanding of the relevance of this nucleation pathway nor any measurements of such contrails. In this study, we have thus used the simplified modification of Gierens (2021), shown in Eq. (4). ~~Here, $\bar{c}_p$ is a~~ We make use of the mol-based ~~mean~~ heat capacity of the exhaust gases ~~(see Eq. (15) of Gierens, 2021), which is not a constant, but we nevertheless define to be 30.6 J/mol/K~~ $\overline{c_p}$, which Gierens (2021) showed not to be a constant (see their Eq. (15)). Nevertheless, we assume it to be $30.6\,\text{J mol}^{-1}\,\text{K}^{-1}$ for all pressure levels for simplicity. This is possible because the variability of the heat capacity is low. ~~η_E~~ We further define the electric efficiency ~~, η_0 is~~ η_E, the basic efficiency ~~and Δh_m~~ η_0 and the formation enthalpy of water vapour Δh_m. For simplicity we combine the two efficiencies into a single efficiency η, as in Table 1.

$$G_{\underline{H_2FC}\,\text{H}_2\text{FC}} = \frac{\bar{c}_p p_a}{(1-\eta_E\eta_0)|\Delta h_m|} \frac{\overline{c_p} p_a}{(1-\eta_E\eta_0)|\Delta h_m|} \tag{4}$$

~~For any given mixing line slope G, we can define two threshold temperatures T_{min} and T_{max} to aid in determining where persistent contrails form. Consider the mixing line shown in blue in Figure 1 for $G = 3.7$ Pa/K, which is tangential to the water vapour saturation curve. T_{max}, sometimes also written Θ (e.g. Kärcher et al., 2015), refers to the temperature at which this threshold mixing line touches the water vapour saturation curve, in this case around 240.1 K; T_{min} refers to the temperature at which the mixing line reaches a water vapour partial pressure of 0 Pa, in this case around 229.9 K. Both values increase with increasing G. The original approximation of T_{max} by Schumann (1996) was extended by Gierens (2021) for higher temperatures (233 to 293 K) and higher mixing line slopes ($G > 2$ Pa/K),~~

$$T_{max} = \begin{cases} 226.69 + 9.43\ln(G - 0.053) + 0.72\left(\ln(G - 0.053)\right)^2 & \text{for } T < 233\,K \text{ or } G \leq 2\,Pa/K \\ 226.03 + 10.22\ln G + 0.335\left(\ln G\right)^2 + 0.0642\left(\ln G\right)^3 & \text{for } G > 2\,Pa/K \end{cases}$$

To determine whether a persistent contrail forms at a given location, we check the following three conditions, which we define as *limiting factors*:

1) *droplet formation* - ambient temperature less than the threshold temperature ($T < T_{max}$ see below) and ambient water vapour partial pressure above the threshold mixing line;

2) *droplet freezing* - ambient temperature less than the homogeneous freezing temperature (235.15 K);

3) *persistence* - ambient water vapour partial pressure above the ice saturation curve.

If these three conditions are all met, a persistent contrail forms. For completeness, a fourth boundary, water supersaturation, can also be defined. However, for the pressure levels of interest in this article, the occurrence of these conditions is insignificant (Krämer et al., 2009). The limiting factors are shown graphically in Figure 1.

To aid in determining droplet formation, we can define two threshold temperatures T_{min} and T_{max}. Consider first the ambient conditions represented by the green square marker (229 K, 10.9 Pa) and the corresponding dashed blue mixing line for $G = 1.9\,\mathrm{Pa\,K^{-1}}$ in Figure 1. For these ambient conditions, an aircraft with a mixing line slope less than $G = 1.9\,\mathrm{Pa\,K^{-1}}$ would not produce a contrail since the mixture never becomes supersaturated with respect to water. The temperature T_{max}, or sometimes Θ (e.g. Kärcher et al., 2015), thus traditionally refers to the temperature at which the threshold mixing line ($G = 1.9\,\mathrm{Pa\,K^{-1}}$) is tangent to the water saturation curve, in this case around 232.7 K (black cross marker). The temperature T_{min} refers to the temperature at which the threshold mixing line has a water vapour partial pressure of 0 Pa, in this case around 223.2 K.

However, we argue that this definition of T_{max} is insufficient for aircraft with higher mixing line slopes. In order for a contrail to form, droplet formation and droplet freezing must occur concurrently. If, using the standard definition, T_{max} is found to be larger than 235.15 K (which occurs for $G > 2.38\,\mathrm{Pa\,K^{-1}}$), it is possible that the plume becomes subsaturated with respect to water again before it cools below 235.15 K. There is thus insufficient time in the plume for ice crystals to form before the water droplets evaporate (see e.g. Figure 3 of Bier et al., 2024). This effect has been described as a reduction in the "effective freezing temperature" because ice crystal numbers reduce as the ambient temperature approaches 235.15 K (Kärcher, 2018; Bier et al., 2022, 2024).

To counter this problem, for aircraft with $G > 2.38\,\mathrm{Pa\,K^{-1}}$, we set the threshold mixing line to intersect with the point of water saturation at the homogeneous freezing temperature - see the blue threshold mixing line for $G = 6.0\,\mathrm{Pa\,K^{-1}}$ in Figure 1. By doing so, we ensure that all possible mixing lines for the ambient conditions within the green hatched area are at some point concurrently supersaturated with respect to water and colder than the homogeneous freezing temperature. Using this method, we are able to closely replicate the ambient temperatures at which Bier et al. (2022) and Bier et al. (2024) find final ice crystal numbers of zero (their Figures 5(c) and 4 respectively) - see Figure S1. In this study, we therefore extend the original approximation of T_{max} by Schumann (1996) and the amendment for higher temperatures by Gierens (2021) to,

$$
T_{max} = \begin{cases}
226.69 + 9.43\ln\left(G - 0.053\right) + 0.72\left(\ln\left(G - 0.053\right)\right)^2 & \text{for } T < 233 \text{ K or } G \leq 2 \text{ Pa K}^{-1} \\
226.03 + 10.22\ln G + 0.335\left(\ln G\right)^2 + 0.0642\left(\ln G\right)^3 & \text{for } 2.38 \text{ Pa K}^{-1} \geq G > 2 \text{ Pa K}^{-1} \\
235.15 & \text{for } G > 2.38 \text{ Pa K}^{-1}
\end{cases}
\tag{5}
$$

2.2 Aircraft definitions

For the limiting factors analysis, we define a range of aircraft, representative of different propulsion technologies. This is necessary to limit required computational resources, but nevertheless allows for a good comparison between the technologies. We ~~selected eight~~ select ten aircraft-fuel combinations that span a range of G from 0.48 to 15.8 Pa~~/K~~ K^{-1} at 250 hPa (Table 1). ~~The reference aircraft CON-LG corresponds to the last generation of~~ We define four conventional, kerosene-powered aircraft ~~, for which we assume an~~ as CON-XX, where XX is the overall propulsion system efficiency η ~~of 0.3. The next generation of kerosene-powered aircraft CON-NG has an improved~~ in percent: 30 % for the previous generation, 37 % for the current state-of-the-art, 40 % for the next generation and 43 % for the future generation. We note that there are a wide range of conventional aircraft currently operating and that the overall propulsion system efficiency ~~of 0.4, therefore a colder exhaust and a higher G. We also~~ varies with the operating condition, altitude and a multitude of other factors. Assuming a single value for comparison is thus not optimal, but necessary for this analysis. Unless otherwise stated, we use CON-37 as the reference aircraft in this study.

We further define an 80 % parallel hybrid-electric aircraft HYB-80. We use a high degree of electrification to differentiate it from the conventional aircraft - a 60 % ~~hybrid~~ hybrid-electric aircraft would have approximately the same mixing line slope as ~~CON-LG~~CON-30. We further include two potential aircraft designs that reduce the effective emission index of water vapour EI_{H_2O} using the Water-Enhanced Turbofan (WET) concept. In this study, we assume for simplicity a reduction in EI_{H_2O} of 50 % (WET-50) and 75 % (WET-75). We ignore the impact of any potential ~~liquid droplets in the plume~~emissions of stored, liquid water that is released outside of ice supersaturated regions (ISSRs). We also define three different hydrogen-powered aircraft: ~~H2C-04~~ H2C-40 is a hydrogen combustion (H$_2$C) aircraft, which assumes $\eta = 0.4$; H2FC-LV and H2FC-HV are hydrogen fuel cell (H$_2$FC) aircraft which ~~operate at~~ have operating voltages of 0.5 and 1.0 V respectively. The operating voltage has a very large influence on the slope of the mixing line, as Gierens (2021) showed. ~~However, we only consider H2C-04 in this analysis, as explained hereafter.~~

~~With the definition of the homogeneous freezing temperature at 235 K, we can calculate a mixing line slope that is tangential to the water saturation curve and crosses the intersection of the ice saturation curve with the homogeneous freezing temperature. Using the Newton method, we find this slope to be $G_{lim} = 4.29$ Pa/K. This mixing line slope is the theoretical limit case: For $G > 4.29$ Pa/K, whether a contrail forms or not is no longer aircraft design dependent, but purely depends on the ambient conditions. H2C-04 has a mixing line slope lower than 4.29 Pa/K only at altitudes higher than 217 hPa; H2FC-LV higher than 205 hPa; and H2FC-HV always has a mixing line slope greater than 4.29 Pa/K. Since it is very unlikely that fuel cell~~

Table 1. Definition of aircraft-engine-fuel combinations used in this study, representative of different current and future propulsion technologies. See text for the description of the variables. The results for the aircraft IDs in brackets are available at the linked data source, but have not ~~further considered~~ been presented in this study~~: H2C-04 is used as a proxy~~'s results for ~~all hydrogen-powered aircraft in this study since all have G higher than~~ the ~~limit case sake~~ of ~~4.29 Pa/K, as described in the main text~~brevity.

Aircraft ID	Description	Eq.	c_p	EI_{H_2O}	Q or Δh	η	G (250 hPa)
WET-75	-75% EI~~H,OH2O~~	(1)	1004 J ~~kg/K~~ kg⁻¹ K⁻¹	0.31 ~~kg/kg~~ kg⁻¹	43.6 ~~e6 J/kg~~ MJ kg⁻¹	~~0.4~~ 0.40	0.48 ~~Pa~~ K⁻¹
(WET-50)	-50% EI~~H,OH2O~~	(1)	1004 J ~~kg/K~~ kg⁻¹ K⁻¹	0.63 ~~kg/kg~~ kg⁻¹	43.6 ~~e6 J/kg~~ MJ kg⁻¹	~~0.4~~ 0.40	0.97 ~~Pa~~ K⁻¹
HYB-80	~~Hybrid (80%)~~ hybrid-electric	(2)	1004 J ~~kg/K~~ kg⁻¹ K⁻¹	1.25 ~~kg/kg~~ kg⁻¹	43.6 ~~e6 J/kg~~ MJ kg⁻¹	0.4 (K), 0.8 (E)	1.15 ~~Pa~~ K⁻¹
~~CON-LG~~ CON-30	~~Last gen. JA1~~ Prev. gen. CON	(1)	1004 J ~~kg/K~~ kg⁻¹ K⁻¹	1.25 ~~kg/kg~~ kg⁻¹	43.6 ~~e6 J/kg~~ MJ kg⁻¹	~~0.3~~ 0.30	1.65 ~~Pa~~ K⁻¹
~~CON-NG~~ CON-37	~~Next gen. JA1~~ Current gen. CON	(1)	1004 J ~~kg/K~~ kg⁻¹ K⁻¹	1.25 ~~kg/kg~~ kg⁻¹	43.6 ~~e6 J/kg~~ MJ kg⁻¹	~~0.4~~ 0.37	1.84 ~~Pa~~ K⁻¹
CON-40	Next gen. CON	(1)	1004 J kg⁻¹ K⁻¹	1.25 kg kg⁻¹	43.6 MJ kg⁻¹	0.40	1.93 Pa K⁻¹
~~H2C-04~~ (CON-43)	Future gen. CON	(1)	1004 J kg⁻¹ K⁻¹	1.25 kg kg⁻¹	43.6 MJ kg⁻¹	0.43	2.03 Pa K⁻¹
H2C-40	H2C	(3)	1004 J ~~kg/K~~ kg⁻¹ K⁻¹	8.94 ~~kg/kg~~ kg⁻¹	120.9 ~~e6 J/kg~~ MJ kg⁻¹	~~0.4~~ 0.40	4.97 ~~Pa~~ K⁻¹
(H2FC-LV)	H₂FC ∼0.5V	(4)	30.6 J ~~/mol/K~~ mol⁻¹ K⁻¹	-	-241.82 kJ ~~/mol~~ mol⁻¹	~~0.4~~ 0.40	5.27 ~~Pa~~ K⁻¹
(H2FC-HV)	H₂FC ∼1.0V	(4)	30.6 J ~~/mol/K~~ mol⁻¹ K⁻¹	-	-241.82 kJ ~~/mol~~ mol⁻¹	~~0.8~~ 0.80	15.8 ~~Pa~~ K⁻¹

215 ~~aircraft will fly at these altitudes and, as we show in our results (cf. Figure 6), persistent contrail formation is not aircraft design dependent at high altitudes, in this study H2C-04 is used as a proxy for all hydrogen-powered aircraft.~~

2.3 Air traffic data

We use a representative future air traffic scenario to weight our results and identify areas of particular interest. In this study, we use the progressive scenario of the DLR internal project *Development Pathways for Aviation up to 2050* ~~(DEPA 2050, Leipold et al., 2021)~~
220 (DEPA 2050, Leipold et al., 2021). A key objective of this project was to define and assess the development of the aviation industry until the year 2050 from multiple angles, including climate, economics and society. It also studied the potential entry into service of various novel aviation fuels and technologies. This scenario was selected for this research since it is representative of a future multi-fuel global fleet and because there are no restrictions on its publication. ~~The~~ We use the forecasted aggregate yearly fuel and distance flown by the global fleet of aircraft in the year 2050 from the DEPA 2050 progressive scenario~~for~~
225 ~~the year 2050 is~~, which is available with a 1° latitude resolution. The emission inventory is included in the linked data and is shown graphically in ~~Supplementary Figure 1.~~ Figure S2.

2.4 ERA5 data and corrections

To calculate regions of potential persistent contrail formation we use the European Centre for Medium-Range Weather Forecasts' (ECMWF) ~~ERA5 reanalysis data (Hersbach et al., 2020)~~ fifth generation reanalysis dataset (ERA5, Hersbach et al., 2020)
230 stored on the German Climate Computing Center's (DKRZ) supercomputer Levante. Specifically, we use the ambient temperature and relative humidity at pressure levels 350, 300, 250, 225, 200, 175 and 150 hPa within the 2010 decade (December 2009 to November 2019 inclusive). In this study, we use RHi to denote relative humidity with respect to ice and RHw to denote relative humidity with respect to water. We further define the seasons ~~Winter, Spring, Summer and Autumn~~ as DJF, MAM,

JJA ~~,~~ and SON respectively. To avoid autocorrelation and reduce the computational time, whilst still obtaining a climatological response, we randomly select 2160 hours per season over the 10-year time frame - this corresponds to 10 % of all hourly values within the 2010 decade. We use *numpy.random.choice* with seed 42 without replacement to determine which hours to choose per season for repeatability. ~~Supplementary Figure 2~~ Figure S3 shows the hours that were selected.

The ERA5 HRES temperature and relative humidity values are archived on a reduced Gaussian grid with a resolution of N320. The pre-interpolated data is available on DKRZ Levante as daily GRIB files. We decided to use the irregular N320 grid for our analysis, rather than interpolated data, to avoid any artefacts of interpolation in the relative humidity data in particular. However, this complicates the definition of cell neighbours and the calculation of the limiting factors, as described in the next section.

Numerous authors have shown the difficulty of estimating ice supersaturated regions (ISSRs) and hence contrail persistence with reanalysis data. For example, Agarwal et al. (2022) found that ERA5 could overestimate ISSR coverage when compared to radiosonde measurements, whereas Reutter et al. (2020) found an underestimation in comparison to in situ IAGOS measurements (Petzold et al., 2015). Gierens et al. (2020), comparing ERA5 with MOZAIC data (Marenco et al., 1998), found that although contrail formation can be predicted reliably, persistence cannot. In a follow-up study, Hofer et al. (2024b) found that even using ~~further ERA5 variables~~ variables other than the relative humidity, ISSR prediction cannot yet be significantly improved.

There have been many suggestions on how to correct ERA5 data to more accurately estimate ISSRs, both at a regional ~~(Wang et al., 2024; Teoh et al., 2022a)~~ (Teoh et al., 2022a; Wang et al., 2024) and global scale ~~(?Hofer et al., 2024b; Teoh et al., 2024)~~ (Hofer et al., 2024b; Teoh et al., 2024; Wolf et al., 2025). In this study, we enhance the ERA5 humidity by applying a correcting factor of $1/RHi_{c_{cor}}$ for $RHi_{c_{cor}} \in \{1.0, 0.98, 0.95, 0.90\}$, as in previous studies ~~(e.g. Schumann, 2012; Teoh et al., 2020; Schumann et al., 2~~ (e.g. Schumann, 2012; Teoh et al., 2020; Reutter et al., 2020; Schumann et al., 2021). We note that this approach does not consider a latitude-dependence of the ERA5 RHi error (Teoh et al., 2024). However, modifying the cumulative distribution function found for ERA5 by Hofer et al. (2024b, their Figure 4) to include the RHi enhancements, we find that $RHi_{c_{cor}} = 0.95$ provides a good fit against MOZAIC/IAGOS data for $RHi \leq 1.0$ (~~Supplementary Figure 3~~Figure S4), which is of relevance for this study. We further discuss the regional implications of this method in Section 3.6.

Previous studies have shown that, compared to IAGOS, ERA5 generally underestimates ambient temperatures, which are also important for determining potential persistent contrail formation regions. At conventional pressure levels, Wolf et al. (2025) find an average global underestimation of up to -0.7 K (see their Figure 3). At higher altitudes (lower pressure levels), the global average difference increases to around -1.0 K. We analysed the impact of a global increase of 0.1, 0.5 and 1.0 K on climatological potential persistent contrail formation (cf. Sections 2.7 & 3.4) and found that the effect of the temperature bias is small compared to that of relative humidity (see Figure S7). Therefore, we do not consider the temperature correction any further in this study and focus on sensitivities with respect to relative humidity.

2.5 Limiting factors analysis

The objective of the limiting factors analysis is to understand the aircraft design-, altitude-, latitude- and seasonal dependence of the factors responsible for persistent contrail formation. This helps us identify regions where the introduction of aircraft using novel propulsion systems and fuels with substantially higher mixing line slopes, e.g. hydrogen combustion, would lead to increased persistent contrail formation. Or, where the use of aircraft with substantially lower mixing line slopes, such as hybrid-electric or WET aircraft, could be particularly beneficial.

We first consider the probability of persistent contrail formation p_{pcf} for each aircraft design. This is calculated by creating a boolean mask for persistent contrail formation using the three limiting factors for all 3D grid cells, time steps and aircraft designs. The boolean values for each grid cell are averaged and saved per month. Since the underlying ERA5 grid is irregular, when reporting and analysing a global p_{pcf}, we use an area- and level-weighting. We calculate the area of all grid cells as viewed from above using the *calculate_areas* method of the Python library *scipy.spatial.SphericalVoronoi* with an assumed spherical Earth radius of 6371 km and assume the cell areas to be constant with altitude. Since ERA5 also has irregular spacing in altitude, we use the difference (in hPa) between pressure levels to level-weight the results.

We then consider each limiting factor individually. For each aircraft design, time step and grid cell, we determine which of the limiting factors prevent a persistent contrail from forming. By summing the number of times each factor was limiting and normalising by the number of time steps, we obtain the probability of each limiting factor preventing persistent contrail formation. The results are saved per season-year (e.g. 2010 DJF) to limit memory usage. We ~~can~~ then investigate the dependence of each limiting factor on altitude, latitude and season. When reporting global results, we perform area- and level-weighting as before.

2.6 Analysis of persistent contrail formation region boundaries

We now consider again Figure 1: If an aircraft is flying with the mixing line slope G shown by the blue line in ambient conditions within the green hatched area, a persistent contrail will form. If the ambient conditions are subsequently no longer within the green hatched area, due to changes in the ambient temperature, relative humidity, altitude or in aircraft performance, the aircraft will stop producing a persistent contrail, thus defining the boundary of a persistent contrail formation region. One or more of the limiting factors will have been responsible for that boundary.

The objective of this analysis is to understand the relative importance of the limiting factors in defining the horizontal and vertical boundaries of persistent contrail formation regions. In the horizontal direction, we begin by calculating the total perimeter of all persistent contrail formation regions. Then, we compare the length of the boundary caused by each limiting factor to the total perimeter. The boundary lengths for each limiting factor are thus subsets of the total. But since multiple factors can be simultaneously limiting, the sum of all limiting factor boundary lengths is greater than the total. A large boundary length for a given limiting factor means that that factor was often responsible for persistent contrails forming.

We demonstrate this analysis graphically in an example shown in Figure 2 for H2C-40 using fictional data on the ERA5 grid for a single time and pressure level over the Netherlands. ~~For a given aircraft design, green cloud icon nodes represent~~
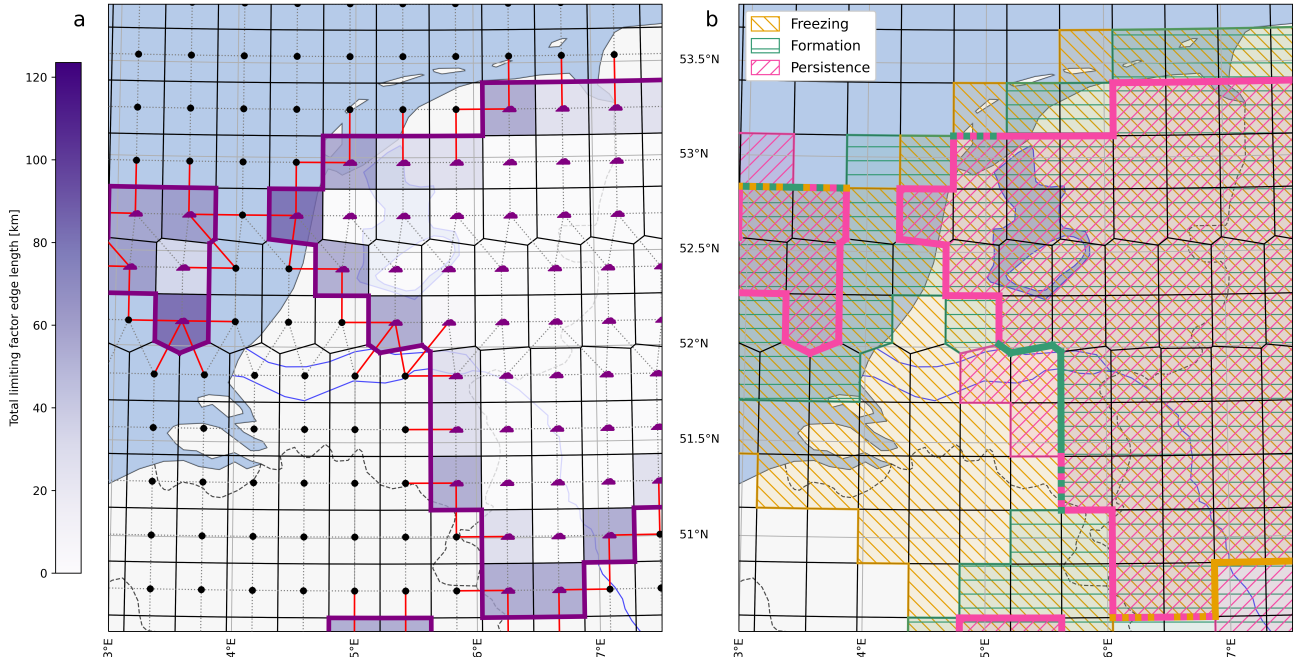
11

Figure 2. Example of the horizontal ~~total~~ limiting factors analysis for ~~a hydrogen combustion aircraft (H2C-04)~~ H2C-40 using fictional data at a single ~~time (February 11th, 2024 at 08:00 UTC) at a single~~ pressure level ~~(300 hPa)~~ over the Netherlands~~as calculated with ERA5 without RHi correction. Persistent~~ **(a)** Analysis of the total limiting factor - persistent contrails would form ~~for this aircraft~~ at all grid points with a ~~green~~ purple cloud icon. The ~~thick green~~ red lines correspond to all possible boundary crossings into the ~~edge of the~~ potential persistent contrail formation regions; the ~~red lines to all possible boundary crossings; and the~~ purple shading to the length of the ~~persistent contrail~~ boundary around each grid cell. **(b)** Droplet freezing (yellow hatching), droplet formation ~~region~~ (green hatching) and persistence (pink hatching) limiting factors. The thick coloured lines represent which limiting factor is responsible for the boundary. If multiple factors are responsible, the line is dashed. For the analysis of each limiting factor individually, only the correspondingly coloured boundaries are considered in the edge length around each grid cell.

~~grid points where a persistent contrail would form; black points where none are expected.~~ We calculate the borders between
300   grid cells (~~solid~~ black lines) using the *scipy.spatial. SphericalVoronoi* method ~~,~~ and find cell neighbours (gray dotted lines) by determining which cells share a pair of edge vertices. The combination of persistence, droplet freezing and droplet formation (coloured hatching) results in potential persistent contrail formation regions (purple cloud icons). We are interested in the boundaries of persistent contrail formation regions, therefore we need to identify neighbouring cells with different icons (red ~~, solid~~ lines). These cells i and j share a border d_{ij} (thick ~~green~~ purple line), which we calculate using the Haversine formula
305   assuming an Earth radius of 6371 km. The colour gradient bar indicates the length of the persistent contrail formation region border around each grid cell: a darker ~~green~~ purple corresponds to a longer boundary, a lighter ~~green~~ purple to a shorter

boundary. By globally summing all d_{ij}, we obtain the total perimeter of all persistent contrail formation regions. This is repeated for the boundaries caused by individual limiting factors (thick yellow, green and pink lines).

Programmatically, for each aircraft design and time step, we create four 3D boolean masks: one for potential persistent contrail formation and one per limiting factor. For each aircraft design, time step, pressure level and limiting factor, we create a global, symmetric adjacency matrix A of size $n \times n$, where $n = 542080$ is the number of grid points in the ERA5 grid. For any two adjacent cells i and j, $A_{ij} = d_{ij}$ (shared border length, thick ~~green~~ purple line) if the persistent contrail formation boolean at i is TRUE (persistent contrail forms, ~~green~~ purple cloud icon) and the limiting factor boolean at j is FALSE (the limiting factor has prevented persistent contrail formation, black point), else $A_{ij} = 0$. To obtain the total perimeter, we set $A_{ij} = d_{ij}$ if *any* limiting factor boolean at j is FALSE. We then obtain the vector of size n of boundary lengths around each grid cell (cell colour gradient) by summing the columns of the adjacency matrix. This procedure is repeated for each time step and the monthly summed values for each aircraft design, grid cell, pressure level and limiting factor are saved ~~to file~~. We repeat the full analysis for all RHi enhancements.

We perform a similar analysis in the vertical direction to analyse the impact of changing altitude and thus mixing line slope G. For simplicity, we neglect the changes in aircraft operating conditions during climb or descent to a new altitude. Vertically ~~neighbouring~~ adjacent cells can be found easily because the latitude-longitude location of the cells is constant with altitude. Since there are no clearly defined edge lengths in the vertical direction, we calculate the boundaries of persistent contrail formation regions by summing the cell areas as viewed from above.

2.7 Maximum slope analysis

In the limiting factors analysis, fixed aircraft designs with specific values of G are used. The objective of this second analysis is to explore the dependence of persistent contrail formation p_{pcf} on G in more detail ~~,~~ and determine whether there is a climatological relationship between the two. We analyse the results at the global level as well as on three latitude-dependent scales: the northern extratropics (latitude > 30°N), the tropics (30°S $\leq$ latitude $\leq$ 30°N) and the southern extratropics (latitude < 30°S).

For each cell where the ambient conditions are sufficient for persistent contrail formation, we use the Newton method to find the slope where the mixing line is tangent to the water saturation curve. ~~The slope of~~ If the temperature at which this mixing line ~~we define as G_{max} - the~~ is tangential to the water saturation curve (T_{max}) is greater than the homogeneous freezing temperature (235.15 K), we set T_{max} to 235.15 K (see Section 2.1). The slope of the line that connects the ambient conditions to the water supersaturated conditions for T_{max} is thus the maximum mixing line slope for which a persistent contrail would not form. We define this threshold mixing line G_{max}. For example, for the ambient conditions shown by a green square in Figure 1 ~~the blue line corresponds to $G_{max} = 3.7$ Pa/K~~, the corresponding maximum slope is $G_{max} = 1.9$ Pa K^{-1} (blue dashed line). For each region, altitude and time step, we use a histogram with a bin size of 0.2 ~~Pa/K~~ Pa K^{-1} to determine the distribution of G_{max}. By taking the cumulative sum of the histograms, we obtain p_{pcf} as a function of G.

3   Results and Discussion

340 This section presents and discusses the results of the limiting factors analyses. Sections 3.1 and 3.2 analyse the limiting factors within each grid cell and at the boundaries of persistent contrail formation regions. The altitude- and latitude-dependence of these regions and the changes in global potential persistent contrail formation p_{pcf} are presented in Section 3.3. In Section 3.4, we develop climatological relationships between the mixing line slope and the p_{pcf}. Finally, we discuss the interplay and competition between the limiting factors in Section 3.5 and the limitations and uncertainties of our study in Section 3.6.

345 ### 3.1   Limiting factors of persistent contrail formation

We find that the formation of persistent contrails is primarily limited by ice supersaturation (persistence limiting factor). Figure 3 shows the global area- and level-weighted potential persistent contrail formation (p_{pcf}) and the frequency that each limiting factor prevented a persistent contrail from forming. Enhancing the area of ice supersaturation by lowering the relative humidity threshold as a means of correcting ERA5 relative humidity (see Sect. 2.4) increases p_{pcf}, proportionally more for
350 aircraft with higher G (markers).

The altitude- and latitude-dependence of the limiting factors is shown in Figure 4. The persistence limiting factor is less limiting in the extratropics at lower altitudes (350 to 250 hPa) and in the tropics at higher altitudes (225 to 150 hPa, see Supplementary Figure 4), but in total). In total, it prevents persistent contrail formation 92.3 % of the time. Enhancing humidity by lowering the threshold for ice supersaturation reduces how limiting persistence is, as expected. On the other hand, droplet
355 freezing is generally only limiting in the tropics at altitudes below FL300 (pressure levels $\geq$ 300 hPa), in total only 18.2 % of the time. It is by definition unaffected by humidity enhancements.

Droplet formation is highly dependent on the slope of the mixing line G and varies between 18.119.2 % (H2C-04H2FC-HV) and 89.5 % (WET-75). It varies insignificantly with enhanced humidity. An interesting finding Interesting to note is that the H2C-04 droplet formation and the droplet results of the H2FC-HV droplet formation limiting factor closely follow those of
360 the aircraft design-independent droplet freezing limiting factor. This is due to our definition of T_{max} at high mixing line slopes (see Section 2.1): The higher the aircraft mixing line slope, the steeper the threshold mixing line slope and thus the closer it resembles the vertical droplet freezing factors are very similar, both in their normalised sum as in their latitude- and altitude-dependence (Supplementary Figure 4). The reason for this is that there is some overlap in the definition of the limiting factors: Ambient conditions that are to the right of the steep mixing line will likely also be to the right of the droplet freezing
365 line . The result is that the droplet formation limiting factor acts like persistence at low G and like droplet freezing at high Glimit at 235.15 K.

3.2   Boundaries of persistent contrail formation regions

Persistence is also found to be more limiting compared to the other factors at the region boundaries. Figure 5 shows the sum over all pressure levels of the horizontal (a) and vertical (b) boundary lengths/areas of potential persistent contrail formation
370 regions as a function of the limiting factor and aircraft design. We show the total in absolute terms and the individual limiting
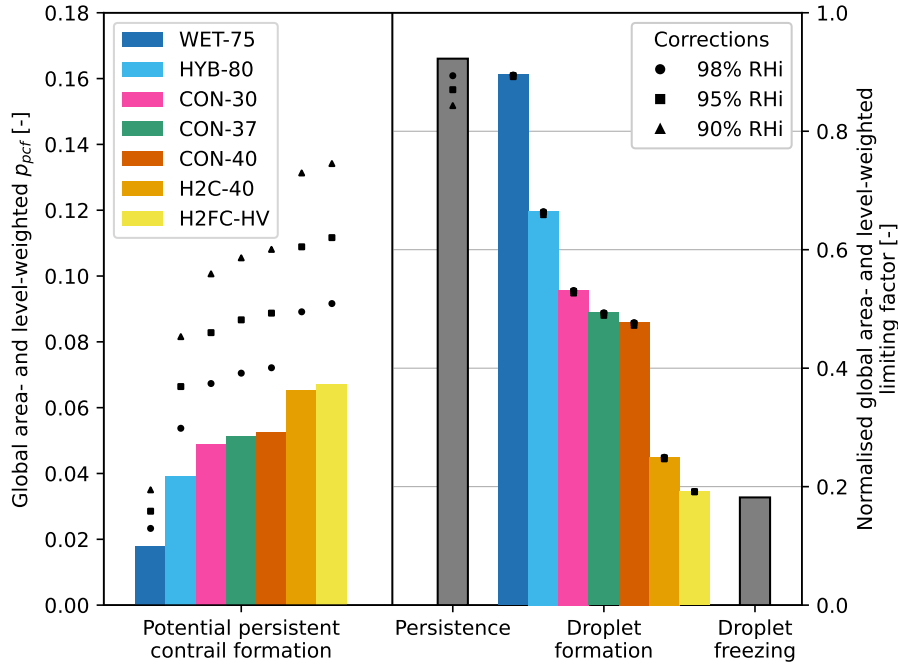
Figure 3. Global area- and level-weighted potential persistent contrail formation during the 2010 decade (left) and the normalised frequency that each limiting factor prevented a persistent contrail from forming (right). A normalised frequency of 0 would mean that the factor never limited persistent contrail formation; 1 that it always does. Dependence on aircraft design is shown by the different colours - the persistence and droplet freezing limiting factors are independent of aircraft design and thus only have single values. The RHi enhancements are shown as scatter points - note the difference in the y-scale.

factors relative to the total for ease of comparison. Because more than one limiting factor may simultaneously be responsible for a boundary, the sum of the individual limiting factors may be larger than 100 %. Since the horizontal and vertical directions cannot be directly compared, we have ~~aligned the~~ visually aligned the y-axes for the CON-37 total limiting factor ~~for CON-LG~~ such that at least the shapes of the responses can be compared. In both cases, the persistence limiting factor dominates for all

375   aircraft designs and increases with increasing G. This is because as G increases, contrails can form in larger proportions of ice supersaturated regions.

     Droplet formation can be limiting when the ambient conditions would be sufficient for persistent contrail formation, but G is sufficiently low that the exhaust does not become supersaturated with respect to water. The droplet formation limiting factor thus becomes less relevant as G increases. ~~In horizontal direction, it is no longer relevant once $G > 4.29$ Pa/K since~~

380   ~~for all ambient conditions conducive to persistent contrail formation the mixing line would cross the water saturation curve.~~ Since G changes with altitude for the same aircraft, ~~in the vertical direction~~ droplet formation is responsible for a significantly
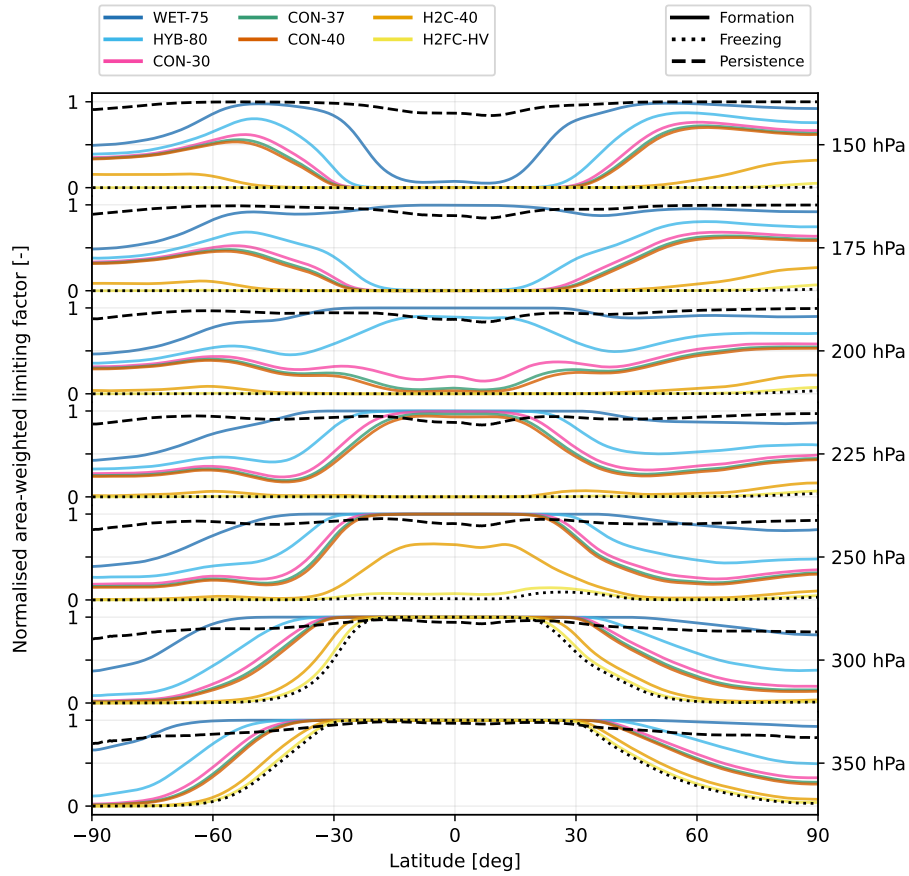
15

Figure 4. Normalised and area-weighted global limiting factors of the 2010 decade as a function of latitude (x-axis) and altitude (secondary y-axis). A normalised frequency of 0 would mean that the factor never limits persistent contrail formation; 1 that it always does. Droplet freezing (dotted lines) and persistence (dashed lines) are independent of aircraft design. Droplet formation is dependent on aircraft design and shown for the different designs (colours).

larger proportion of the persistent contrail formation region boundaries in the vertical direction compared to the horizontal. It is particularly limiting for very low G aircraft such as the WET-75.

In comparison, the droplet freezing limiting factor becomes more important with increasing G. Low mixing line slopes
385   prevent contrails from forming near the freezing boundary. Therefore, droplet freezing is only relevant for aircraft with a high G, in particular hydrogen-powered aircraft. Again due to the changing G with altitude and ~~higher~~ larger change in ambient temperature in ~~vertical than in~~ the vertical compared to the horizontal direction, the droplet freezing limiting factor is also more relevant in the vertical direction.
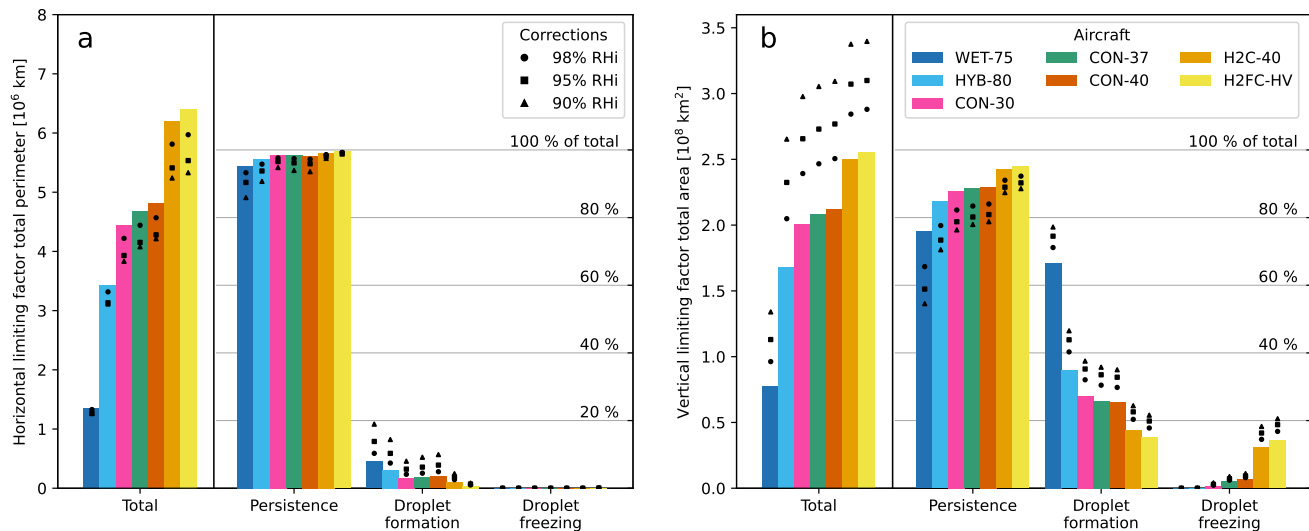
Figure 5. Horizontal (**a**) and vertical (**b**) total limiting factor results. The "total" limiting factors are shown in absolute values, visually aligned for ~~CON-LG~~ CON-37 such that the shapes of the responses can be compared; the individual limiting factors are shown relative to the corresponding total value and are given in percent. Because more than one factor may simultaneously be limiting, the sum of the individual percentages may be larger than 1. The RHi enhancements are shown as scatter points.

The RHi correction does not influence which factor is most limiting, with the single exception of WET-75 in the vertical direction. It also does not, on a climatological timescale, influence in which areas persistent contrails form: As the humidity is enhanced, the probability that a persistent contrail forms increases where the probability was already greater than zero (cf. ~~Supplementary Figure 5~~ Figure S5). However, the persistence results show that many ambient conditions in ERA5 are close to being saturated with respect to ice. Our results thus only add to the consensus that improving ISSR forecasting is vital for estimating persistent contrail formation (Gierens et al., 2020; Hofer et al., 2024b).

In the horizontal direction, enhancing humidity seems to reduce the total edge length, even though the potential persistent contrail formation regions are larger. A significant reduction in edge length can be identified by enhancing humidity by only 2 %, in particular for hydrogen-powered aircraft. This suggests that the potential persistent contrail formation regions, predominantly described by ice supersaturation, grow and coalesce with enhancing humidity, reducing the total length of their boundaries. ~~In~~ Further work would be required to prove this theory. In the horizontal direction, the RHi correction has ~~only a minor~~ a virtually no influence on the droplet freezing, but a major influence on the droplet formation limiting factor. In both cases, however, the ~~total~~ perimeter remains two orders of magnitude smaller than that of the persistence limiting factor. In the vertical direction, enhancing humidity increases the boundary area significantly for the total. Seemingly, the boundary between different pressure levels is emphasised by the enhanced humidity, notably for the droplet formation limiting factor.

17

3.3 Spatial variability of persistent contrail formation

405 The summation of the region edges does not provide any information about where persistent contrails form. Therefore, we now explore the altitude-, latitude- and aircraft-dependence of persistent contrail formation regions. Figure 6(a) shows that aircraft design is only ever limiting at lower altitudes: Except for aircraft with very low mixing line slopes (HYB-80, ~~WET~~WET-75), whether a contrail forms and persists ~~above~~ for pressure levels < 200 hPa (altitudes above FL385) depends solely on the ambient conditions.
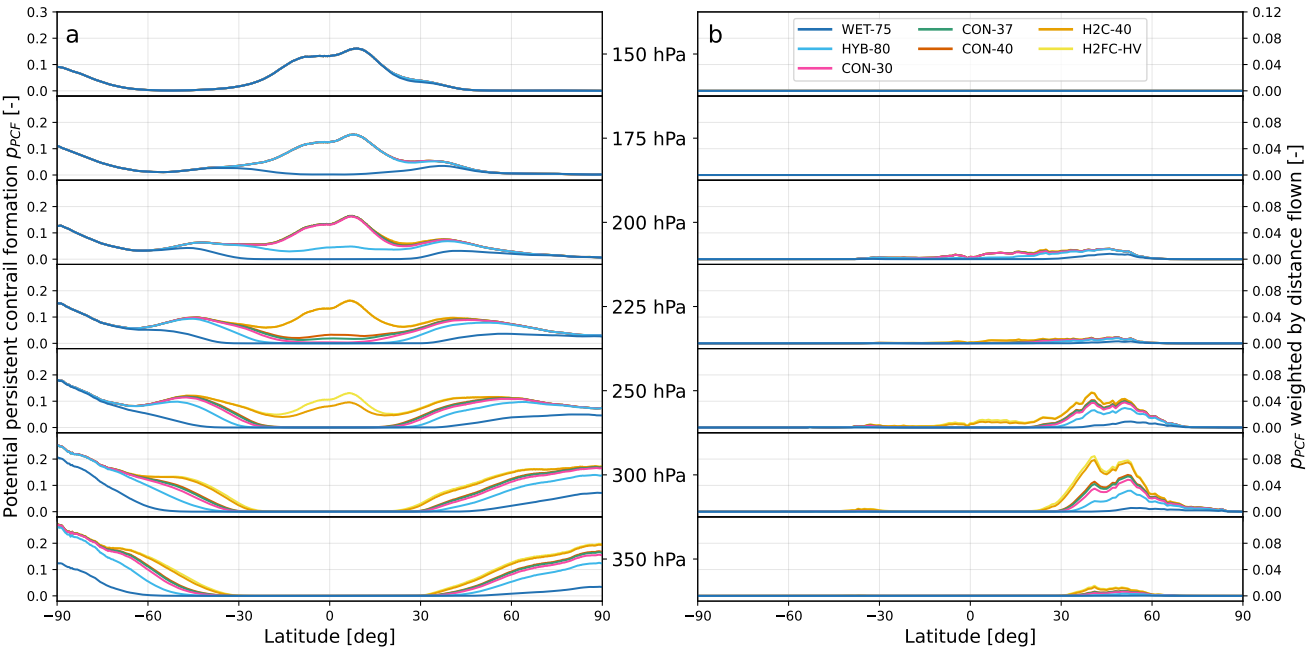

Figure 6. Potential persistent contrail formation p_{pcf} **(a)** as a function of latitude (x-axis) and altitude (secondary y-axis). ~~p_{pcf} is~~ We then ~~weighted~~ weight p_{pcf} by the distance flown in the DEPA 2050 air traffic scenario in the year 2050 **(b)** to identify important areas for persistent contrail formation.

410 It has been widely assumed that the introduction of hydrogen-powered aircraft would result in a significant increase in the formation of persistent contrails. Our results show that ~~a~~ hydrogen-powered aircraft ~~, represented by H2C-04,~~ could indeed form many more persistent contrails than existing conventional aircraft~~(CON-LG). Comparing the two aircraft designs directly.~~ Comparing H2C-40 and H2FC-HV with CON-37, our results match those of Kaufmann et al. (2024, the right side of their Figure 5): At low altitude (350 to 300 hPa), a large difference in persistent contrail formation (Kaufmann et al. (2024) call

415 this "potential contrail cirrus cover") can be seen between 30 to 60°S and 30 to 60°N, incidentally coinciding with significant air traffic over Europe and the US. ~~However, the largest difference occurs in the tropics between 250 and 225 hPa: 17.9 and 5.2 times more persistent contrails could be formed respectively (Supplementary Table 1).~~ In total, across all latitudes and

considered altitudes, hydrogen-powered aircraft have the potential to produce ~~25.7 %~~ between 18.3 % (H2C) and 20.8 % (H2FC) more persistent contrails than conventional aircraft (~~Table 1~~CON-37, see Table S1).

Since these results do not consider where aircraft actually fly, we have also used the DEPA 2050 air traffic scenario to weight the results, as shown in Figure 6(b). DEPA 2050 is only available with a 1° latitude resolution, so we conservatively regrid the limiting factors results to match this resolution (conserving the total sum of distance flown). The tropical increase in persistent contrail formation at ~~225 to~~ 250 to 225 hPa is now less pronounced because there are few aircraft flying in this region. Instead, of particular importance are the northern extratropics between 300 and 250 hPa (FL300 to FL340), which are the lower cruise altitudes for typical airliners. In total, our simple distance-weighted proxy shows a globally-averaged increase of ~~71.4 % (Table 1)~~ 46.5 % to 54.7 % for hydrogen-powered aircraft (H2C and H2FC respectively) compared to conventional aircraft (CON-37, see Table S1). This indicates that replacing existing aircraft along existing and expected flight routes with hydrogen-powered designs would significantly increase persistent contrail formation - on a climatological timescale whilst ignoring any real-time avoidance strategies.

Significant reductions in persistent contrail formation could be gained by reducing the water vapour emission index: globally, WET-50 achieves a ~~23.3~~26.0 % reduction; WET-75 a ~~55.1~~56.6 % reduction. Along the DEPA 2050 flight routes, this further improves to ~~47.2~~51.7 % and ~~83.7~~85.1 % respectively. There is also clearly potential for the targeted introduction of aircraft with very low mixing line slopes, in particular at higher altitudes (225 to 200 hPa, FL360 - ~~FL380~~FL385) in the tropics. Here, the WET aircraft considered would produce little to no persistent contrails at all, with unweighted reductions of ~~83~~83.2 - ~~87~~91.4 % (WET-50) and 99.5 - ~~99.95~~99.96 % (WET-75).

For all aircraft designs, persistent contrail formation increases with altitude in the tropics and decreases in the extratropics, in line with previous studies (e.g. Matthes et al., 2021). Among others, Barton et al. (2023) suggest designing hydrogen-powered aircraft capable of flying at higher altitudes in the extratropics - around 14 km (140 hPa) - to avoid forming persistent contrails. We find that very few persistent contrails are formed at 150 hPa ~~above~~ north of 30°N and between ~~-30~~30°S and ~~-60~~60°S (very few flight tracks extend ~~below -60~~south of 60°S). Since this is due to a lack of ice supersaturation in these regions (see ~~Supplementary Figure 4~~Figure 4), this concept does not need to be limited to hydrogen-powered aircraft. However, these altitudes are above the local tropopause ~~,~~ and releasing significant amounts of water vapour and NO_x into the stratosphere can result in a significant increase in climate impact ~~(Matthes et al., 2021; Grewe et al., 2010)~~(Grewe et al., 2010; Matthes et al., 2021). We therefore stress that these results should not be used in isolation to determine a possible optimum cruise altitude. Rather, the full climate impact of a given design must be considered.

3.4 Climatological potential persistent contrail formation

We now ~~wish~~ aim to determine whether there is a climatological relationship between the mixing line slope G and the potential persistent contrail formation p_{pcf}. Figure 7 shows p_{pcf} as a function of ~~the mixing line slope~~ G for each pressure level and for all data together, without RHi enhancement. The results for all RHi enhancements are shown in ~~Supplementary Figure 6. An asymptote in the data at $G_{lim} =$~~ Figure ~~4.29 Pa/K exists by definition (see Section 2.2), but for~~ S6. The supremum value for each pressure level and time can be determined by ignoring the droplet formation limiting factor, since it resembles the droplet freezing limiting factor as $G \to \infty$. For many pressure levels, 99 % of that ~~maximum value is actually~~ supremum value is achieved at much lower mixing line slopes ($G_{99\%sup}$ in Table 2 and black circular markers in Figure 7). Generally, the higher the altitude, the earlier the results asymptote and the less influence the aircraft design has. This also matches the results found in Figure 6.

For very low G, persistent contrails form only at very high altitude. As G increases, more persistent contrails are formed at lower altitudes ~~. The altitude~~ (higher pressure levels). The pressure levels with the highest p_{pcf} is likely between 250 and 225 hPa (FL340 - FL360) at $G >$ ~~4 Pa/K~~ 7 Pa K^{-1}. For these two ~~altitudes~~ pressure levels in particular, the results seem to be the addition of two different responses. We find that the initial slope is the extratropical response (both northern and southern) ~~,~~ and the second slope the tropical response (right side of Figure 7). Given the higher tropopause and ambient temperature in the tropics, persistent contrails generally form at higher values of G compared to the extratropics.

We fit the responses using the sum of two logistic functions, one representing the response from the tropics and the other from the extratropics. A conventional logistic function includes the supremum L, the growth rate k and the midpoint of the growth x_0, with limits 0 for $x \to -\infty$ and L for $x \to +\infty$. We have allowed the extratropical logistic function to be shifted vertically by d for a better fit, noting that the fitting function is only valid for $G > 0$ Pa~~/K~~ K^{-1}. To find the optimal parameters, we consider the tropical logistic function to be an addition to the extratropical function. Therefore, we split the data into two at a certain value of G~~and~~ : We use the values of G up until this split to create the extratropical response ~~,~~ and the values after the split to create the tropical response. We subsequently use a minimisation function to determine the best value for the split.

$$f(x) = \frac{L_1}{1 + e^{-k_1(x - x_{0,1})}} + \frac{L_2}{1 + e^{-k_2(x - x_{0,2})}} + d \tag{6}$$

The result is that the value of the maximum for the full equation can be read as $L_1 + L_2 + d$. For the ~~altitudes~~ pressure levels 175 and 150 hPa, we find that there is no need to use a second logistic function because persistent contrails do not form at these ~~altitudes~~ pressures in the extratropics. For these ~~altitudes~~ pressure levels, therefore, the value of the asymptote is simply $L + d$. ~~Since there is by definition an asymptote at $G_{lim} = 4.29$ Pa/K, we only grouped values of G up until $G = 4.5$ Pa/K. To help the minimisation function describe the asymptotic behaviour above this limit value, we artificially extended the results to 6.5 Pa/K. This is represented as the faded part of Figure 7.~~

The parameters found by the minimisation function are shown in Table 2. We generally find a good fit and a high coefficient of determination (R^2), except for 150 hPa and all level data together. At 150 hPa, the seasonal responses reach an asymptote at a very low G, such that the response is essentially horizontal and thus by definition cannot have a good R^2 value. By considering
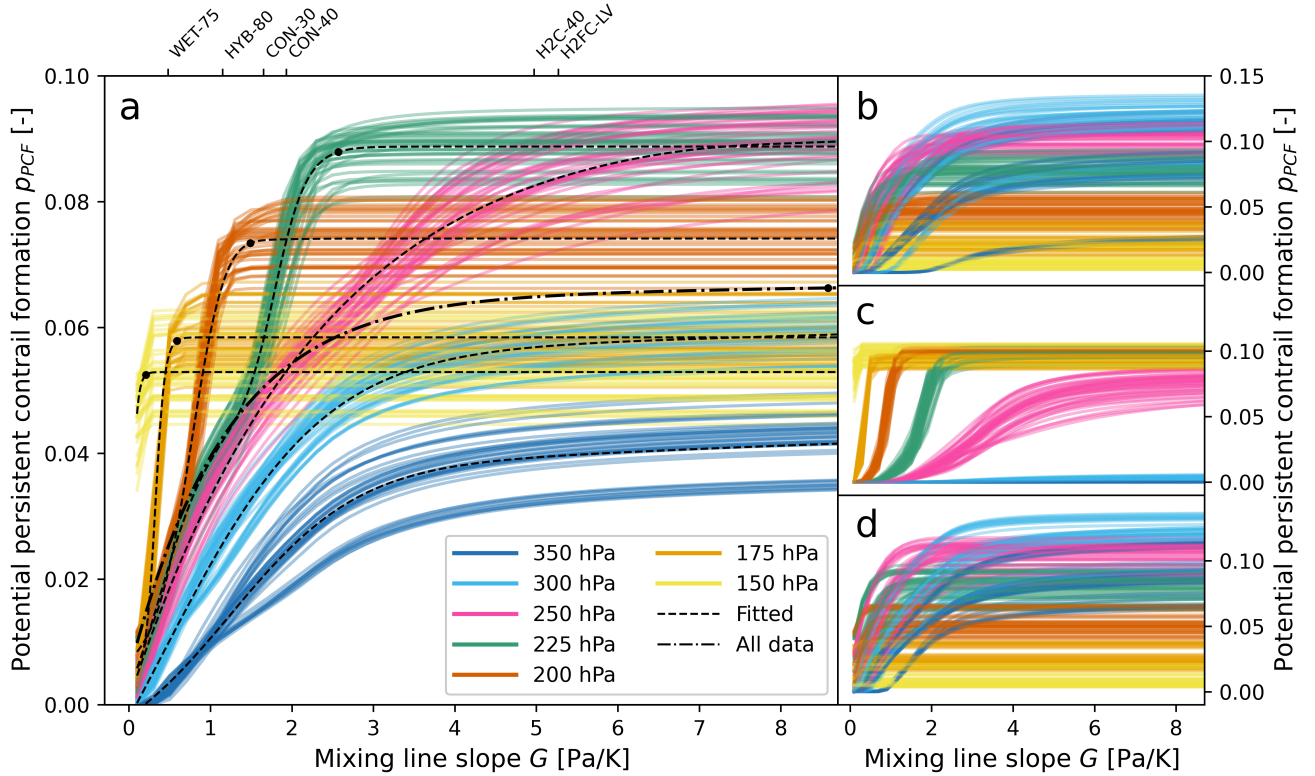
Figure 7. Potential persistent contrail formation p_{pcf} as a function of the mixing line slope G on a climatological timescale for pressure levels 350 to 150 hPa **(a)** at a global scale and for **(b)** the northern extratropics, **(c)** the tropics and **(d)** the southern extratropics. Each coloured line corresponds to a single season within the 2010 decade. The dashed lines are the fitted responses using the modified logistic function in Eq. (6) and parameters as defined in Table 2, for each pressure level individually ("fitted") and for all pressure levels together ("all data"). The ~~faded part for $G > 4.29$ Pa/K represents where the data was extended to improve the accuracy of the fits (see main text for more details). The~~ markers show at which value of G the corresponding p_{pcf} reaches within 1 % of the supremum. The mixing line slopes of the different aircraft designs are shown for the pressure level 250 hPa for reference.

all level data together, the differentiation between the extratropical and tropical responses are essentially no longer visible. The R^2 value is thus not high, clearly showing that including level information is beneficial in determining p_{pcf}. We note that the

485   "all data" response in Figure 7 has a similar shape to the gentle sloping curve in Figure 2 of Hofer et al. (2024a), who consider persistent contrail formation from potential SAF aircraft using IAGOS/MOZAIC data, irrespective of the altitude.

    As Figure 3 demonstrated, p_{pcf} increases with enhanced relative humidity because more ambient conditions, in particular closer to the freezing temperature limit, are conducive to persistent contrail formation. The same analysis as above is conducted for all RHi enhancements and shown in ~~Supplementary Figure 6.~~ <u>Figure S6.</u> The fitted results are stretched to higher p_{pcf}

490   but maintain the same general shape, including the marked difference in the extratropical and tropical responses. This again

Table 2. Optimal parameters for potential persistent contrail formation p_{pcf} as a function of the mixing line slope G (Eq. 6) on a climatological timescale for pressure levels 350 to 150 hPa and for all pressure levels together ("all data"). ~~$L+d$ corresponds to the maximum~~ The supremum value ~~,~~ of the function $L+d$ is shown ~~in~~ as a percentage. For each pressure level, the top values of L, k and x_0 are for the first logistic function (extratropical response) and the bottom values for the second logistic function (tropical response). The pressure levels 175 and 150 hPa are primarily driven by the tropical response (cf. Figure 7) and thus did not benefit from the second logistic function. The variable $G_{99\%sup}$ corresponds to the lowest value of G for which the corresponding p_{pcf} is within 1 % of the supremum $L+d$.

Level	~~L~~ L	~~k~~ k	~~x_0~~ x_0	~~d~~ d	~~$L+d$~~ $L+d$ [%]	R^2	$G_{99\%sup}$ [~~Pa/K~~ K^{-1}]
All data	~~0.167~~9.001 ~~0.010~~0.001	~~1.35~~0.84 ~~2.00~~0.51	~~-0.578~~-5.92 ~~2.78~~8.12	~~-0.109~~-8.936	~~6.77~~6.70	~~0.446~~0.253	~~4.32~~8.58
350 hPa	~~0.040~~0.049 ~~0.010~~0.004	~~1.63~~1.24 ~~2.99~~0.48	~~1.21~~1.24 ~~3.24~~7.07	~~-0.006~~-0.011	~~4.41~~4.28	~~0.937~~0.846	~~4.49~~11.63
300 hPa	~~0.082~~0.100 ~~0.011~~0.003	~~1.24~~1.00 ~~2.49~~0.53	~~0.47~~0.39 ~~2.97~~8.60	~~-0.032~~-0.043	~~6.16~~6.02	~~0.978~~0.946	~~4.66~~10.94
250 hPa	~~0.107~~2.072 ~~0.031~~-0.002	~~1.37~~0.45 ~~3.70~~1.87	~~0.21~~-6.86 ~~3.14~~7.76	~~-0.046~~-1.979	~~9.26~~9.13	~~0.985~~0.958	~~4.26~~10.40
225 hPa	0.055 0.044	3.17 ~~5.15~~5.13	0.38 ~~1.79~~1.80	-0.010	~~8.87~~8.88	~~0.981~~0.954	2.57
200 hPa	0.077 -0.007	4.32 ~~5.16~~5.14	0.78 1.38	0.005	7.41	~~0.957~~0.891	1.49
175 hPa	0.054	17.3	0.32	0.005	5.84	~~0.865~~0.680	0.59
150 hPa	~~0.318~~0.237	~~24.6~~24.5	~~-0.05~~-0.04	~~-0.266~~-0.185	5.29	~~0.050~~0.018	0.21

suggests that, on a climatological timescale, as relative humidity is enhanced, the probability that a persistent contrail forms increases where the probability was already greater than zero (cf. ~~Supplementary Figure 5~~Figure S5).

3.5   Competition between limiting factors

We find that for all aircraft designs, persistence is the most limiting factor and most responsible for the borders of persistent contrail formation regions (Figures 3 and 5 respectively). At first glance, this seems counterintuitive: Persistence is independent of aircraft design, ~~and yet~~ but the size of the potential persistent contrail formation regions do depend on the aircraft design and vary significantly. In this section, we discuss the interplay and competition between the different limiting factors.

Consider the analysis of persistent contrail formation regions in the horizontal direction for ~~the H2C-04~~H2FC-HV, a high-G aircraft. Since most region boundaries are defined by persistence and we do not change the operating condition of the aircraft between grid cells, the difference between two neighbouring cells must therefore mostly be a slight increase in relative humidity - a vertical shift in Figure 1. If we lower G, both neighbouring cells could then be to the right of the limiting slope, preventing

a persistent contrail from forming in the cell that is supersaturated with respect to ice and thus also preventing the border. In this case, our analysis does not recognise formation being limiting because the formation boundary was not crossed. If we now consider a horizontally contiguous ice supersaturated region and an arbitrary aircraft then this implies that this aircraft will or will not form a contrail, independently of where it crosses the region boundary. Furthermore, at high values of G, the limiting slope acts much like a vertical boundary. Indeed, the ~~freezing and H2C-04~~ droplet freezing and H2FC-HV droplet formation limiting factors show very similar results (cf. Figure 3 and ~~Supplementary Figure 4~~Figure 4).

How ~~then to view~~ should the competition between the persistence and droplet formation limiting factors be viewed? The persistence and droplet freezing limiting factors together create an upper bound to the potential persistent contrail formation region size. The droplet formation limiting factor then controls what proportion of this region is available for persistent contrails to form. Figure 7 shows that the level of control varies with latitude and altitude: at high altitudes, aircraft design has barely any influence.

3.6 Uncertainties and limitations

As with all climatological analyses and models, there are a number of limitations in the usage of our results. For example, consider the latitude-dependent results in Figure 7. In theory, more information could be gained by including two distinct extratropical and tropical responses. No persistent contrails are produced in the tropics at 350 hPa and essentially none are produced at 300 hPa, but if the globally averaged fits were to be used, persistent contrails would be assumed to form in these regions. However, the results in the individual latitude bands also have a higher seasonal dependence (notably in the tropics at 250 hPa). There is thus a trade-off in the level of detail that can be included if persistent contrail formation is to be climatologically modelled. Clearly, it would be inappropriate to analyse the climate impact of an aviation scenario that only considers aircraft flying in one latitude region using the globally fitted responses. Similarly, it would also be inappropriate to use the fits to analyse aircraft flying only in a single season. Instead, our results are useful for global aviation or aircraft-specific scenarios with a time step of at least one year.

It is also important to underline the difference between persistent contrail formation and the resulting contrail cirrus coverage and climate impact. The results presented in this study are valid only for static persistent contrail formation, i.e. do not consider contrail spreading or temporal changes in the local ambient conditions: We assume a contrail to be persistent if the ambient conditions are supersaturated with respect to ice at the time of formation, however since the water vapour field is highly heterogeneous and can vary rapidly with time, the contrail may not actually persist. We are not able to consider dynamic conditions such as the subsidence of the local air mass that may lead to contrail sublimation. It is also possible that persistent contrails formed in one grid cell spread to neighbouring cells due to mixing. Particularly interesting are neighbouring cells that are limited by the droplet formation limiting factor, i.e. are themselves not conducive for persistent contrail formation, but are supersaturated with respect to ice and are below the homogeneous freezing temperature. In a previous study, these regions were defined as "reservoirs" for persistent contrails (Wolf et al., 2023). ~~Due to the vertical or horizontal spreading of contrails with time, it is thus possible that persistent contrails can nevertheless form~~ As contrails spread vertically and/or horizontally over time, they may persist in grid cells that our analysis ~~found to be~~ identified as limited by droplet formation. Such spreading

is certainly important for the calculation of a contrail cirrus coverage, but since it is a secondary, dynamic effect we have not included it in this study on persistent contrail formation.

Care should also be taken when using our results to inform aircraft design or flight trajectories. For example, we show that replacing kerosene with hydrogen along assumed future flight trajectories could result in ~~71.4~~around 50 % more persistent contrails (cf. Table ~~1~~S1) on a climatological timescale without considering contrail avoidance strategies. This does not, however, translate to a ~~71.4~~50 % larger radiative forcing or temperature change due to differing contrail properties. For example, Rap et al. (2023) find a 70 % increase in contrail coverage from hydrogen-powered aircraft compared to conventional aircraft, ~~largely in line with our results,~~ but also find a 25 % reduction in contrail cirrus Effective Radiative Forcing (ERF). Similar results were found by Grewe et al. (2017a). Persistent contrail formation should thus not be used as a direct proxy for climate impact ~~,~~and more research is required into contrail properties from novel aviation fuels and propulsion technologies. We also reiterate that contrails are only part of the equation and that the full climate impact, including other non-CO_2 effects, should be used to inform aircraft design or flight trajectories.

The globally averaged, climatological results presented in this study are not expected to change significantly due to a changing climate. Our results show that persistence is the most limiting factor for all aircraft designs. Therefore, the probability of persistent contrail formation should vary in tandem with the frequency and location of ISSRs. Climate models predict a generally warmer upper troposphere and generally cooler lower stratosphere, leading to a decrease in relative humidity in the tropics and an increase towards ~~to poles (Benetatos et al., 2024; Irvine and Shine, 2015)~~the poles (Irvine and Shine, 2015; Benetatos et al., 2024). This is reflected in the results of both ~~Bock and Burkhardt (2019) and Chen and Gettelman (2016)~~ Chen and Gettelman (2016) and Bock and Burkhardt (2019), who find for a future atmosphere a decrease in the probability of persistent contrail formation (here p_{pcf}) in the tropics and an increase in the northern extratropics. Chen and Gettelman (2016) find a net reduction in contrail cirrus radiative forcing, whereas Bock and Burkhardt (2019) expect the radiative forcing to approximately even out.

If the global p_{pcf} remains approximately the same, then the limiting factor results (Figure 5) and the competition between the limiting factors should also remain unchanged. However, the regional differences in ISSR location may modify the shape of the responses in Figure 7, lowering the maximum p_{pcf} values in the tropics and raising them in the extratropics. For the pressure levels 250 to 200 hPa, which are driven by both a tropical and extratropical response, the global result will likely have a steeper initial slope and a shallower secondary slope, shifted slightly to higher mixing line slopes. Nevertheless, the maximum values and the general shape of the responses are not expected to change significantly.

Finally, we do not expect the choice of global aviation scenario to have significantly affected the weighted results. In this study, we used the DEPA 2050 progressive scenario for the year 2050 since it is representative of a future multi-fuel global fleet and due to its ease of publication. Other global scenarios may produce slightly different weighted results, but the focus should nevertheless remain on the northern extratropics at 300-250 hPa.

4 Conclusions

Persistent contrail formation is limited by three main factors: droplet formation, droplet freezing and persistence. Our investigation using ERA5 data in the 2010 decade finds persistence (ice supersaturation) to be the most limiting factor. Of the considered grid cells, 92.3 % are not supersaturated with respect to ice and thus not conducive to persistent contrail formation. Droplet freezing is found to be limiting 18.2 % of the time and droplet formation between ~~18.1~~19.2 % (~~hydrogen-powered aircraft~~high voltage hydrogen fuel cell) and 89.5 % (Water Enhanced Turbofan with 75 % water vapour reduction). The boundaries of persistent contrail formation regions are also generally defined by the persistence limiting factor, regardless of aircraft design. In other words, should an aircraft - without changing its operating condition - start producing a persistent contrail, generally it is because the air mass it has entered is supersaturated with respect to ice. Our results thus underscore the importance of accurately estimating ice supersaturated regions (Gierens et al., 2020; Hofer et al., 2024b).

We demonstrate the feasibility of developing high-quality climatological relationships between the mixing line slope G and the potential persistent contrail formation p_{pcf} for individual pressure levels. We create these relationships using the sum of two modified logistic functions, one representing the response from the tropics and the other from the extratropics. The combination of the persistence and droplet freezing limiting factors create an upper bound for the size of persistent contrail formation regions, which varies by latitude, altitude and season. We find that~~using the standard Schmidt-Appleman Criterion, aircraft design can no longer limit persistent contrail formation for mixing line slopes $G > 4.29$ Pa/K. However,~~, due to the distribution of ice supersaturation with altitude, ~~the actual limit is generally lower and decreases with altitude. Therefore, the higher the altitude, the less influence the aircraft design has.~~ aircraft design becomes less limiting with increasing altitude (decreasing pressure level). For very low G, persistent contrails form only at very high altitude. As G increases, more persistent contrails are also formed at lower altitudes. These climatological relationships are the first step in the development of a computationally inexpensive method to analyse the contrail climate impact of novel aviation fuels and propulsion technologies on a climatological timescale.

Novel aviation fuels and propulsion technologies will have a major impact on persistent contrail formation. Across all considered flight levels, improving overall propulsion efficiency from ~~0.3 to 0.4~~0.30 to 0.40 increases persistent contrail formation by ~~13.8~~13.6 % along representative flight trajectories~~. Replacing all aircraft by~~; from 0.37 to 0.40 by 4.0 %. A significant reduction in persistent contrail formation could be achieved using a water vapour emission reduction system such as the Water Enhanced Turbofan concept - up to 85.1 % by reducing the water vapour emission index by 75 % compared to a reference conventional aircraft with an overall propulsion system efficiency of 0.37. On the other hand, compared to the same reference aircraft, hydrogen combustion or fuel cell aircraft could result in a ~~71.4~~46.5 to 54.7 % increase ~~. We note~~respectively. It is, however, ~~that persistent~~ important to keep in mind which aircraft is taken as reference - an overall propulsion system efficiency of 0.37 is representative of current state-of-the-art, but likely higher than the global average. Compared to the global average, the increase may be even higher.

Persistent contrail formation, as analysed here, is not synonymous with contrail climate impact. Contrails produced by aircraft using alternative fuels such as hydrogen are expected to have very different optical and radiative properties. Although such

aircraft may produce significantly more persistent contrails, their overall contrail climate impact may in fact be lower than conventional aircraft ~~(Bier et al., 2024; Rap et al., 2023; Gierens, 2021)~~(Gierens, 2021; Rap et al., 2023; Bier et al., 2024). More research is required to better understand this effect. ~~On the other hand, the Water Enhanced Turbofan concept could reduce persistent contrail formation by 53.6 % to 85.6 % along expected flight trajectories (WET-50/WET-75 vs. CON-NG). Our~~

605 ~~results , therefore,~~ Nevertheless, our results point to a clear potential for the targeted introduction of aircraft with low mixing line slopes to significantly reduce persistent contrail formation.

610 *Author contributions.* Conceptualisation: L.M. and V.G.; Methodology, investigation and visualisation: L.M.; Supervision: V.G.; Original draft: L.M.; Review and editing: L.M. and V.G. Both authors read and approved the final manuscript.

Competing interests. The authors declare no competing interests.

References

Agarwal, A., Meijer, V. R., Eastham, S. D., Speth, R. L., and Barrett, S. R. H.: Reanalysis-Driven Simulations May Overestimate Persistent Contrail Formation by 100%–250%, Environmental Research Letters, 17, 014 045, https://doi.org/10.1088/1748-9326/ac38d9, 2022.

Appleman, H.: The Formation of Exhaust Condensation Trails by Jet Aircraft, Bulletin of the American Meteorological Society, 34, 14–20, https://doi.org/10.1175/1520-0477-34.1.14, 1953.

Barton, D. I., Hall, C. A., and Oldfield, M. K.: Design of a Hydrogen Aircraft for Zero Persistent Contrails, Aerospace, 10, 688, https://doi.org/10.3390/aerospace10080688, 2023.

Benetatos, C., Eleftheratos, K., Gierens, K., and Zerefos, C.: A Statistically Significant Increase in Ice Supersaturation in the Atmosphere in the Past 40 Years, Scientific Reports, 14, 24 760, https://doi.org/10.1038/s41598-024-75756-9, 2024.

Bier, A. and Burkhardt, U.: Variability in Contrail Ice Nucleation and Its Dependence on Soot Number Emissions, Journal of Geophysical Research: Atmospheres, 124, 3384–3400, https://doi.org/10.1029/2018JD029155, 2019.

Bier, A., Unterstrasser, S., and Vancassel, X.: Box Model Trajectory Studies of Contrail Formation Using a Particle-Based Cloud Microphysics Scheme, Atmospheric Chemistry and Physics, 22, 823–845, https://doi.org/10.5194/acp-22-823-2022, 2022.

Bier, A., Unterstrasser, S., Zink, J., Hillenbrand, D., Jurkat-Witschas, T., and Lottermoser, A.: Contrail Formation on Ambient Aerosol Particles for Aircraft with Hydrogen Combustion: A Box Model Trajectory Study, Atmospheric Chemistry and Physics, 24, 2319–2344, https://doi.org/10.5194/acp-24-2319-2024, 2024.

Bock, L. and Burkhardt, U.: Contrail Cirrus Radiative Forcing for Future Air Traffic, Atmospheric Chemistry and Physics, 19, 8163–8174, https://doi.org/10.5194/acp-19-8163-2019, 2019.

Bräuer, T., Voigt, C., Sauer, D., Kaufmann, S., Hahn, V., Scheibe, M., Schlager, H., Diskin, G. S., Nowak, J. B., DiGangi, J. P., Huber, F., Moore, R. H., and Anderson, B. E.: Airborne Measurements of Contrail Ice Properties—Dependence on Temperature and Humidity, Geophysical Research Letters, 48, e2020GL092 166, https://doi.org/10.1029/2020GL092166, 2021a.

Bräuer, T., Voigt, C., Sauer, D., Kaufmann, S., Hahn, V., Scheibe, M., Schlager, H., Huber, F., Le Clercq, P., Moore, R. H., and Anderson, B. E.: Reduced Ice Number Concentrations in Contrails from Low-Aromatic Biofuel Blends, Atmospheric Chemistry and Physics, 21, 16 817–16 826, https://doi.org/10.5194/acp-21-16817-2021, 2021b.

Brock, C. A., Froyd, K. D., Dollner, M., Williamson, C. J., Schill, G., Murphy, D. M., Wagner, N. J., Kupc, A., Jimenez, J. L., Campuzano-Jost, P., Nault, B. A., Schroder, J. C., Day, D. A., Price, D. J., Weinzierl, B., Schwarz, J. P., Katich, J. M., Wang, S., Zeng, L., Weber, R., Dibb, J., Scheuer, E., Diskin, G. S., DiGangi, J. P., Bui, T., Dean-Day, J. M., Thompson, C. R., Peischl, J., Ryerson, T. B., Bourgeois, I., Daube, B. C., Commane, R., and Wofsy, S. C.: Ambient Aerosol Properties in the Remote Atmosphere from Global-Scale in Situ Measurements, Atmospheric Chemistry and Physics, 21, 15 023–15 063, https://doi.org/10.5194/acp-21-15023-2021, 2021.

Burkhardt, U. and Kärcher, B.: Global Radiative Forcing from Contrail Cirrus, Nature Climate Change, 1, 54–58, https://doi.org/10.1038/nclimate1068, 2011.

Burkhardt, U., Bock, L., and Bier, A.: Mitigating the Contrail Cirrus Climate Impact by Reducing Aircraft Soot Number Emissions, npj Climate and Atmospheric Science, 1, 37, https://doi.org/10.1038/s41612-018-0046-4, 2018.

Caiazzo, F., Agarwal, A., Speth, R. L., and Barrett, S. R. H.: Impact of Biofuels on Contrail Warming, Environmental Research Letters, 12, 114 013, https://doi.org/10.1088/1748-9326/aa893b, 2017.

Chen, C.-C. and Gettelman, A.: Simulated 2050 Aviation Radiative Forcing from Contrails and Aerosols, Atmospheric Chemistry and Physics, 16, 7317–7333, https://doi.org/10.5194/acp-16-7317-2016, 2016.

655 Filippone, A.: Assessment of Aircraft Contrail Avoidance Strategies, Journal of Aircraft, 52, 872–877, https://doi.org/10.2514/1.C033176, 2015.

Gierens, K.: Theory of Contrail Formation for Fuel Cells, Aerospace, 8, 164, https://doi.org/10.3390/aerospace8060164, 2021.

Gierens, K., Lim, L., and Eleftheratos, K.: A Review of Various Strategies for Contrail Avoidance, The Open Atmospheric Science Journal, 2, 1–7, https://doi.org/10.2174/1874282300802010001, 2008.

660 Gierens, K., Matthes, S., Rohs, S., and Susanne Rohs: How Well Can Persistent Contrails Be Predicted, Aerospace, 7, 169, https://doi.org/10.3390/aerospace7120169, 2020.

Grewe, V., Plohr, M., Cerino, G., Muzio, M. D., Deremaux, Y., Galerneau, M., Martin, P. d. S., Chaika, T., Hasselrot, A., Tengzelius, U., and Korovkin, V. D.: Estimates of the Climate Impact of Future Small-Scale Supersonic Transport Aircraft – Results from the HISAC EU-project, The Aeronautical Journal, 114, 199–206, https://doi.org/10.1017/S000192400000364X, 2010.

665 Grewe, V., Champougny, T., Matthes, S., Frömming, C., Brinkop, S., Søvde, O. A., Irvine, E. A., and Halscheidt, L.: Reduction of the Air Traffic's Contribution to Climate Change: A REACT4C Case Study, Atmospheric Environment, 94, 616–625, https://doi.org/10.1016/j.atmosenv.2014.05.059, 2014.

Grewe, V., Bock, L., Burkhardt, U., Dahlmann, K., Gierens, K., Hüttenhofer, L., Unterstrasser, S., Rao, A. G., Bhat, A., Yin, F., Reichel, T. G., Paschereit, O., and Levy, Y.: Assessing the Climate Impact of the AHEAD Multi-Fuel Blended Wing Body, Meteorologische Zeitschrift,
670 26, 711–725, https://doi.org/10.1127/metz/2016/0758, 2017a.

Grewe, V., Dahlmann, K., Flink, J., Frömming, C., Ghosh, R., Gierens, K., Heller, R., Hendricks, J., Jöckel, P., Kaufmann, S., Kölker, K., Linke, F., Luchkova, T., Lührs, B., Van Manen, J., Matthes, S., Minikin, A., Niklaß, M., Plohr, M., Righi, M., Rosanka, S., Schmitt, A., Schumann, U., Terekhov, I., Unterstrasser, S., Vázquez-Navarro, M., Voigt, C., Wicke, K., Yamashita, H., Zahn, A., and Ziereis, H.: Mitigating the Climate Impact from Aviation: Achievements and Results of the DLR WeCare Project, Aerospace, 4, 34,
675 https://doi.org/10.3390/aerospace4030034, 2017b.

Grewe, V., Matthes, S., Frömming, C., Brinkop, S., Jöckel, P., Gierens, K., Champougny, T., Fuglestvedt, J., Haslerud, A., Irvine, E., and Shine, K.: Feasibility of Climate-Optimized Air Traffic Routing for Trans-Atlantic Flights, Environmental Research Letters, 12, 034 003, https://doi.org/10.1088/1748-9326/aa5ba0, 2017c.

Haywood, J. M., Allan, R. P., Bornemann, J., Forster, P. M., Francis, P. N., Milton, S., Rädel, G., Rap, A., Shine, K. P., and Thorpe, R.:
680 A Case Study of the Radiative Forcing of Persistent Contrails Evolving into Contrail-induced Cirrus, Journal of Geophysical Research: Atmospheres, 114, 2009JD012 650, https://doi.org/10.1029/2009JD012650, 2009.

Hersbach, H., Bell, B., Berrisford, P., Hirahara, S., Horányi, A., Muñoz-Sabater, J., Nicolas, J., Peubey, C., Radu, R., Schepers, D., Simmons, A., Soci, C., Abdalla, S., Abellan, X., Balsamo, G., Bechtold, P., Biavati, G., Bidlot, J., Bonavita, M., De Chiara, G., Dahlgren, P., Dee, D., Diamantakis, M., Dragani, R., Flemming, J., Forbes, R., Fuentes, M., Geer, A., Haimberger, L., Healy, S., Hogan, R. J.,
685 Hólm, E., Janisková, M., Keeley, S., Laloyaux, P., Lopez, P., Lupu, C., Radnoti, G., De Rosnay, P., Rozum, I., Vamborg, F., Villaume, S., and Thépaut, J.-N.: The ERA5 Global Reanalysis, Quarterly Journal of the Royal Meteorological Society, 146, 1999–2049, https://doi.org/10.1002/qj.3803, 2020.

Hofer, S., Gierens, K., and Rohs, S.: Contrail Formation and Persistence Conditions for Alternative Fuels, Meteorologische Zeitschrift, p. 104105, https://doi.org/10.1127/metz/2024/1178, 2024a.

690 Hofer, S., Gierens, K., and Rohs, S.: How Well Can Persistent Contrails Be Predicted? An Update, Atmospheric Chemistry and Physics, 24, 7911–7925, https://doi.org/10.5194/acp-24-7911-2024, 2024b.

Irvine, E. A. and Shine, K. P.: Ice Supersaturation and the Potential for Contrail Formation in a Changing Climate, Earth System Dynamics, 6, 555–568, https://doi.org/10.5194/esd-6-555-2015, 2015.

Kaiser, S., Schmitz, O., Ziegler, P., and Klingels, H.: The Water-Enhanced Turbofan as Enabler for Climate-Neutral Aviation, Applied Sciences, 12, 12 431, https://doi.org/10.3390/app122312431, 2022.

Kärcher, B.: Formation and Radiative Forcing of Contrail Cirrus, Nature Communications, 9, 1824–1824, https://doi.org/10.1038/s41467-018-04068-0, 2018.

Kärcher, B. and Yu, F.: Role of Aircraft Soot Emissions in Contrail Formation, Geophysical Research Letters, 36, L01 804, https://doi.org/10.1029/2008GL036649, 2009.

Kärcher, B., Burkhardt, U., Bier, A., Bock, L., and Ford, I. J.: The Microphysical Pathway to Contrail Formation, Journal of Geophysical Research: Atmospheres, 120, 7893–7927, https://doi.org/10.1002/2015JD023491, 2015.

Kaufmann, S., Dischl, R., and Voigt, C.: Regional and Seasonal Impact of Hydrogen Propulsion Systems on Potential Contrail Cirrus Cover, Atmospheric Environment: X, 24, 100 298, https://doi.org/10.1016/j.aeaoa.2024.100298, 2024.

Krämer, M., Schiller, C., Afchine, A., Bauer, R., Gensch, I., Mangold, A., Schlicht, S., Spelten, N., Sitnikov, N., Borrmann, S., De Reus, M., and Spichtinger, P.: Ice Supersaturations and Cirrus Cloud Crystal Numbers, Atmospheric Chemistry and Physics, 9, 3505–3522, https://doi.org/10.5194/acp-9-3505-2009, 2009.

Lee, D., Fahey, D., Skowron, A., Allen, M., Burkhardt, U., Chen, Q., Doherty, S., Freeman, S., Forster, P., Fuglestvedt, J., Gettelman, A., De León, R., Lim, L., Lund, M., Millar, R., Owen, B., Penner, J., Pitari, G., Prather, M., Sausen, R., and Wilcox, L.: The Contribution of Global Aviation to Anthropogenic Climate Forcing for 2000 to 2018, Atmospheric Environment, 244, 117 834, https://doi.org/10.1016/j.atmosenv.2020.117834, 2021.

Leipold, A., Aptsiauri, G., Ayazkhani, A., Bauder, U., Becker, R.-G., Berghof, R., Claßen, A., Dadashi, A., Dahlmann, K., Dzikus, N., Flüthmann, N., Grewe, V., Göhlich, L., Grimme, W., Günther, Y., Jaksche, R., Jung, M., Knabe, F., Kutne, P., Le Clercq, P., Pabst, H., Poggel, S., Staggat, M., Wicke, K., Wolters, F., Zanger, J., and Zill, T.: DEPA 2050 – Development Pathways for Aviation up to 2050 (Final Report), Berichtsreihe, 2021.

Marenco, A., Thouret, V., Nédélec, P., Smit, H., Helten, M., Kley, D., Karcher, F., Simon, P., Law, K., Pyle, J., Poschmann, G., von Wrede, R., Hume, C., and Cook, T.: Measurement of Ozone and Water Vapor by Airbus In-service Aircraft: The MOZAIC Airborne Program, an Overview, Journal of Geophysical Research: Atmospheres, 103, 25 631–25 642, https://doi.org/10.1029/98JD00977, 1998.

Matthes, S., Lim, L., Burkhardt, U., Dahlmann, K., Dietmüller, S., Grewe, V., Haslerud, A. S., Hendricks, J., Owen, B., Pitari, G., Righi, M., and Skowron, A.: Mitigation of Non-CO2 Aviation's Climate Impact by Changing Cruise Altitudes, Aerospace, 8, 36, https://doi.org/10.3390/aerospace8020036, 2021.

Meerkötter, R., Schumann, U., Doelling, D. R., Minnis, P., Nakajima, T., and Tsushima, Y.: Radiative Forcing by Contrails, Annales Geophysicae, 17, 1080–1094, https://doi.org/10.1007/s00585-999-1080-7, 1999.

Moore, R. H., Thornhill, K. L., Weinzierl, B., Sauer, D., D'Ascoli, E., Kim, J., Lichtenstern, M., Scheibe, M., Beaton, B., Beyersdorf, A. J., Barrick, J., Bulzan, D., Corr, C. A., Crosbie, E., Jurkat, T., Martin, R., Riddick, D., Shook, M., Slover, G., Voigt, C., White, R., Winstead, E., Yasky, R., Ziemba, L. D., Brown, A., Schlager, H., and Anderson, B. E.: Biofuel Blending Reduces Particle Emissions from Aircraft Engines at Cruise Conditions, Nature, 543, 411–415, https://doi.org/10.1038/nature21420, 2017.

Petzold, A., Thouret, V., Gerbig, C., Zahn, A., Brenninkmeijer, C. A. M., Gallagher, M., Hermann, M., Pontaud, M., Ziereis, H., Boulanger, D., Marshall, J., Nédélec, P., Smit, H. G. J., Friess, U., Flaud, J.-M., Wahner, A., Cammas, J.-P., Volz-Thomas, A., and Team, I.: Global-

Scale Atmosphere Monitoring by in-Service Aircraft – Current Achievements and Future Prospects of the European Research Infrastructure IAGOS, Tellus B: Chemical and Physical Meteorology, 67, 28 452, https://doi.org/10.3402/tellusb.v67.28452, 2015.

Pouzolz, R., Schmitz, O., and Klingels, H.: Evaluation of the Climate Impact Reduction Potential of the Water-Enhanced Turbofan (WET) Concept, Aerospace, 8, 59, https://doi.org/10.3390/aerospace8030059, 2021.

Rap, A., Feng, W., Forster, P., Marsh, D., and Murray, B.: The Climate Impact of Contrails from Hydrogen Combustion and Fuel Cell Aircraft, https://doi.org/10.5194/egusphere-egu23-5520, 2023.

Reutter, P., Neis, P., Rohs, S., and Sauvage, B.: Ice Supersaturated Regions: Properties and Validation of ERA-Interim Reanalysis with IAGOS in Situ Water Vapour Measurements, Atmospheric Chemistry and Physics, 20, 787–804, https://doi.org/10.5194/acp-20-787-2020, 2020.

Rojo, C., Vancassel, X., Mirabel, P., Ponche, J.-L., and Garnier, F.: Impact of Alternative Jet Fuels on Aircraft-Induced Aerosols, Fuel, 144, 335–341, https://doi.org/10.1016/j.fuel.2014.12.021, 2015.

Rosenow, J. and Fricke, H.: Individual Condensation Trails in Aircraft Trajectory Optimization, Sustainability, 11, 6082, https://doi.org/10.3390/su11216082, 2019.

Sanogo, S., Boucher, O., Bellouin, N., Borella, A., Wolf, K., and Rohs, S.: Variability in the Properties of the Distribution of the Relative Humidity with Respect to Ice: Implications for Contrail Formation, Atmospheric Chemistry and Physics, 24, 5495–5511, https://doi.org/10.5194/acp-24-5495-2024, 2024.

Sausen, R., Hofer, S., Gierens, K., Bugliaro, L., Ehrmanntraut, R., Sitova, I., Walczak, K., Burridge-Diesing, A., Bowman, M., and Miller, N.: Can We Successfully Avoid Persistent Contrails by Small Altitude Adjustments of Flights in the Real World?, Meteorologische Zeitschrift, 33, 83–98, https://doi.org/10.1127/metz/2023/1157, 2024.

Schmidt, E.: Die Entstehung von Eisnebel Aus Den Auspuffgasen von Flugmotoren, Schriften der Deutschen Akademie der Luftfahrt-forschung, 5, 1–22, 1941.

Schmitz, O., Klingels, H., and Kufner, P.: Aero Engine Concepts Beyond 2030: Part 1—The Steam Injecting and Recovering Aero Engine, Journal of Engineering for Gas Turbines and Power, 143, 021 001, https://doi.org/10.1115/1.4048985, 2021.

Schumann, U.: On Conditions for Contrail Formation from Aircraft Exhausts, Meteorologische Zeitschrift, 5, 4–23, https://doi.org/10.1127/metz/5/1996/4, 1996.

Schumann, U.: A Contrail Cirrus Prediction Model, Geoscientific Model Development, 5, 543–580, https://doi.org/10.5194/gmd-5-543-2012, 2012.

Schumann, U. and Heymsfield, A. J.: On the Life Cycle of Individual Contrails and Contrail Cirrus, Meteorological Monographs, 58, 3.1–3.24, https://doi.org/10.1175/AMSMONOGRAPHS-D-16-0005.1, 2017.

Schumann, U., Poll, I., Teoh, R., Koelle, R., Spinielli, E., Molloy, J., Koudis, G. S., Baumann, R., Bugliaro, L., Stettler, M., and Voigt, C.: Air Traffic and Contrail Changes over Europe during COVID-19: A Model Study, Atmospheric Chemistry and Physics, 21, 7429–7450, https://doi.org/10.5194/acp-21-7429-2021, 2021.

Teoh, R., Schumann, U., Majumdar, A., and Stettler, M. E. J.: Mitigating the Climate Forcing of Aircraft Contrails by Small-Scale Diversions and Technology Adoption, Environmental Science & Technology, 54, 2941–2950, https://doi.org/10.1021/acs.est.9b05608, 2020.

Teoh, R., Schumann, U., Gryspeerdt, E., Shapiro, M., Molloy, J., Koudis, G., Voigt, C., and Stettler, M. E. J.: Aviation Contrail Climate Effects in the North Atlantic from 2016 to 2021, Atmospheric Chemistry and Physics, 22, 10 919–10 935, https://doi.org/10.5194/acp-22-10919-2022, 2022a.

765 Teoh, R., Schumann, U., Voigt, C., Schripp, T., Shapiro, M., Engberg, Z., Molloy, J., Koudis, G., and Stettler, M. E. J.: Targeted Use of Sustainable Aviation Fuel to Maximize Climate Benefits, Environmental Science & Technology, 56, 17 246–17 255, https://doi.org/10.1021/acs.est.2c05781, 2022b.

Teoh, R., Engberg, Z., Schumann, U., Voigt, C., Shapiro, M., Rohs, S., and Stettler, M. E. J.: Global Aviation Contrail Climate Effects from 2019 to 2021, Atmospheric Chemistry and Physics, 24, 6071–6093, https://doi.org/10.5194/acp-24-6071-2024, 2024.

770 Ungeheuer, F., Caudillo, L., Ditas, F., Simon, M., Van Pinxteren, D., Kılıç, D., Rose, D., Jacobi, S., Kürten, A., Curtius, J., and Vogel, A. L.: Nucleation of Jet Engine Oil Vapours Is a Large Source of Aviation-Related Ultrafine Particles, Communications Earth & Environment, 3, 319, https://doi.org/10.1038/s43247-022-00653-w, 2022.

Voigt, C., Kleine, J., Sauer, D., Moore, R. H., Bräuer, T., Le Clercq, P., Kaufmann, S., Scheibe, M., Jurkat-Witschas, T., Aigner, M., Bauder, U., Boose, Y., Borrmann, S., Crosbie, E., Diskin, G. S., DiGangi, J., Hahn, V., Heckl, C., Huber, F., Nowak, J. B., Rapp, M., Rauch, B., 775 Robinson, C., Schripp, T., Shook, M., Winstead, E., Ziemba, L., Schlager, H., and Anderson, B. E.: Cleaner Burning Aviation Fuels Can Reduce Contrail Cloudiness, Communications Earth & Environment, 2, 114, https://doi.org/10.1038/s43247-021-00174-y, 2021.

Voigt, C., Lelieveld, J., Schlager, H., Schneider, J., Curtius, J., Meerkötter, R., Sauer, D., Bugliaro, L., Bohn, B., Crowley, J. N., Erbertseder, T., Groß, S., Hahn, V., Li, Q., Mertens, M., Pöhlker, M. L., Pozzer, A., Schumann, U., Tomsche, L., Williams, J., Zahn, A., Andreae, M., Borrmann, S., Bräuer, T., Dörich, R., Dörnbrack, A., Edtbauer, A., Ernle, L., Fischer, H., Giez, A., Granzin, M., Grewe, V., Harder, H., 780 Heinritzi, M., Holanda, B. A., Jöckel, P., Kaiser, K., Krüger, O. O., Lucke, J., Marsing, A., Martin, A., Matthes, S., Pöhlker, C., Pöschl, U., Reifenberg, S., Ringsdorf, A., Scheibe, M., Tadic, I., Zauner-Wieczorek, M., Henke, R., and Rapp, M.: Cleaner Skies during the COVID-19 Lockdown, Bulletin of the American Meteorological Society, 103, E1796–E1827, https://doi.org/10.1175/BAMS-D-21-0012.1, 2022.

Wang, Z., Bugliaro, L., Gierens, K., Hegglin, M. I., Rohs, S., Petzold, A., Kaufmann, S., and Voigt, C.: Machine Learning for Improvement of Upper Tropospheric Relative Humidity in ERA5 Weather Model Data, https://doi.org/10.5194/egusphere-2024-2012, 2024.

785 Wilhelm, L., Gierens, K., and Rohs, S.: Meteorological Conditions That Promote Persistent Contrails, Applied Sciences, 12, 4450, https://doi.org/10.3390/app12094450, 2022.

Wolf, K., Bellouin, N., and Boucher, O.: Long-Term Upper-Troposphere Climatology of Potential Contrail Occurrence over the Paris Area Derived from Radiosonde Observations, Atmospheric Chemistry and Physics, 23, 287–309, https://doi.org/10.5194/acp-23-287-2023, 2023.

790 Wolf, K., Bellouin, N., Boucher, O., Rohs, S., and Li, Y.: Correction of ERA5 Temperature and Relative Humidity Biases by Bivariate Quantile Mapping for Contrail Formation Analysis, Atmospheric Chemistry and Physics, 25, 157–181, https://doi.org/10.5194/acp-25-157-2025, 2025.

Yin, F., Grewe, V., and Gierens, K.: Impact of Hybrid-Electric Aircraft on Contrail Coverage, Aerospace, 7, 147, https://doi.org/10.3390/aerospace7100147, 2020.

795 Yu, F., Kärcher, B., and Anderson, B. E.: Revisiting Contrail Ice Formation: Impact of Primary Soot Particle Sizes and Contribution of Volatile Particles, Environmental Science & Technology, 58, 17 650–17 660, https://doi.org/10.1021/acs.est.4c04340, 2024.